Stabilization of a road-train of articulated vehicles

Eric Lucet, Alain Micaelli

Stabilization of a Road-Train of Articulated Vehicles

Eric Lucet*, Alain Micaelli

CEA, LIST, Interactive Robotics Laboratory, Gif-sur-Yvette, F-91191, France

Abstract

This paper deals with the stable navigation of up to eight articulated vehicles, coupled together to form a road-train. Based on kinematic and dynamic models, three control approaches are proposed for dynamic stabilization in road-train configuration, as well as a methodology for setting control gains, using three possible actuators: damper at the vehicle articulation, front steering or rear drive wheels. Implementation on a 3D simulator, representative of the dynamics of the real system with a high degree of fidelity, demonstrates the controller's performance and robustness in critical scenario conditions. Tests are then conducted in real conditions to validate the new strategy.

Keywords: Articulated vehicle road-train; Linear Quadratic Regulator; Dynamic stabilization; ELK-test.

1. Introduction

1.1. Motivation and prior work

As transport to and from city centres is insufficient, due to congestion and other societal aspects, the European Easily diStributed Personal RapId Transit project ([1], [2]) was launched to design a new specific light electric vehicle. This concept of car-sharing was originally conceived in 1969 when Witkar [3] was first deployed in Amsterdam as a self-service electric car. At that time,

*Corresponding author

Email address: eric.lucet@cea.fr, alain.micaelli@cea.fr (Eric Lucet*, Alain Micaelli)

only one car could be driven at a time, which caused problems in redistributing vehicles to charging stations. More recently, Chispa's redistributable public road-train system [4] was proposed for a car-free Madrid in 1996. Empty vehicles are passively towed in groups by a conventional car and their kinematics are different, but the concept is similar. Also, since 2009 EOscc1 and EOscc2 (EO smart connecting car) were designed in Bremen [5] for electric mobility.

Thus, other similar services of electric car sharing already exist [6], but their use remains limited. In particular, an interest of this new concept lies in the fact that up to 8 of those vehicles can be coupled together in a road-train for an efficient fleet redistribution by a single operator seated in the front vehicle. For this purpose, a coupling system is used to couple the vehicles electromechanically. Then, vehicles can communicate through couplings via CAN buses, this type of communication architecture being similar to the one presented by Cheng and Xu [7]. Each vehicle has its own control unit connected to the steering, propulsion, braking and damper actuators to enable the road-train to navigate safely forward and reverse. A main issue is that such a system is naturally unstable. The challenge is to prevent lateral oscillations (swaying) and the roll-over, jackknifing and trajectory drift of the road-train.

Such a system can be compared to a vehicle with trailers, as for example the one proposed by Morin and Samson [8], except that the trailers are not actuated. In addition, proposing a kinematic model for driftless control would be too restrictive for the scenario considered here where dynamic phenomena occur. Another similar system is a vehicular platoon, studied for example by Contet et al. [9] or by Hao and Barooah [10]. But since the vehicles of a platoon are not physically coupled, dynamic phenomena do not propagate between them. The problems are therefore different, because the road-train system has to face the risk of jackknifing, while a platoon has to face the risk of intervehicle collisions. Consequently, this paper is investigating a new global control approach based on a specific dynamic model of the vehicle road-train.

1.2. Approach

The lateral stabilization of a vehicle road-train is a rather complex problem. This is why a progressive approach was chosen by first considering a dynamic system projected in a horizontal 2D plane, in order to specify and tune the first controllers, based on the dynamic 2D model. The control algorithms are based on the theory of linear quadratic regulators, a detailed description of which is given by Larminat [11]. In a second step, after some evaluations on a complete realistic 3D simulator, these controllers are completed to take into account additional dynamics. Only slight controller tuning is required to obtain satisfactory simulation results, without adding any correction terms. Finally, tests in real conditions are carried out to validate this strategy.

1.3. Layout

In this document, kinematic and dynamic models are established for a road-train of articulated vehicles with front steered axle and rear driven wheels in section 2. The model chosen is horizontal plane, roll and pitch are not taken into account. A vertical rotation articulation is located in the centre of each vehicle. This articulation is operated by a damper.
Models are linearized for stabilization control. Then, a linear quadratic regulator algorithm is designed in section 3 so that lateral position constraints are satisfied by the road-train system. The path to be tracked by the following vehicles is defined as a series of segments parameterized by their curvilinear abscissa and curvature. The 3D dynamic simulation environment used for the tests, including the realistic road-train design, is described in section 4. Control algorithms are then validated in simulation and the results are analysed in section 5. Then, real tests were carried out on a dedicated car track. The experimental protocol and results obtained with a road-train of up to five vehicles are presented in Section 6. Finally, conclusions and perspectives are given in section 7.

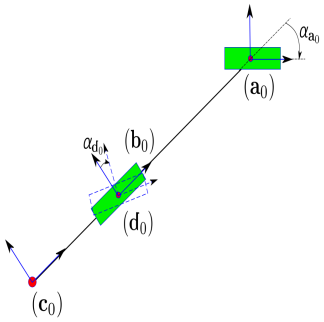

Figure 1: Leader module

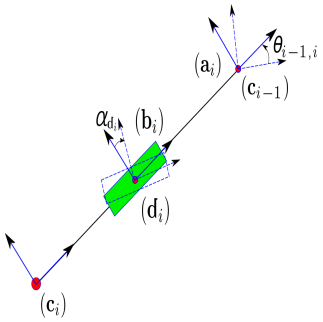

Figure 2: Intermediate module

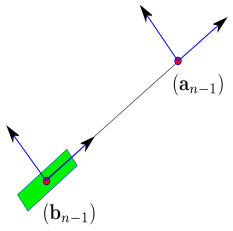

Figure 3: Ender module

2. Road-Train Model

For the design of stabilization control laws, a complex enough 2D model is computed using Lie group theory [12]. On the basis of a reasonable assumption, no elasticity is taken into account, except for road tire contacts. A road-train of vehicles can then be modelized as a serial polyarticulated chain of solid bodies.

2.1. The different modules

All vehicles are composed of two bodies *Front and Rear chassis* articulated around a vertical axis rotation joint. In road-train configuration, the *Front Chassis* of a follower is rigidly coupled to the *Rear Chassis* of the vehicle in front, and all 4 wheels are on the same horizontal axis of rotation. The rotation joint of the first vehicle is locked, so its *Front Chassis* and *Rear Chassis* are aligned, and three different modules have to be considered for the road-train model:

- The Leader module (see Fig. 1): first vehicle *Front Chassis* and *Rear Chassis*, and second vehicle *Front Chassis*;
- The Intermediate module (see Fig. 2): *Front Chassis* of a follower and *Rear Chassis* of the preceding vehicle;
- The Ender module (see Fig. 3): *Rear Chassis* of the last vehicle.

The road-train configuration can be described by the posture of each module such as:

$$\mathbf{h} = \begin{bmatrix} \theta \\ \mathbf{p} \end{bmatrix} \text{ or } \mathbf{H} = \begin{bmatrix} \mathbf{R}_\theta & \mathbf{p} \\ \mathbf{O}_{1\times 2} & 1 \end{bmatrix} \text{ with } \mathbf{R}_\theta = \begin{bmatrix} \cos\theta & -\sin\theta \\ \sin\theta & \cos\theta \end{bmatrix}.$$

θ is the module orientation, $\mathbf{p}$ its 2D position vector, and $\mathbf{R}_\theta$ the θ rotation matrix in the considered frame i. In a more compact and minimal way, the road-train configuration is specified by:

- $\mathbf{h}_0$, for the leader module;
- $\theta_{i-1,i} = \theta_i - \theta_{i-1}$, for the followers, with $1 \leq i \leq n-1$, the module index from leader to ender.

Another information to be considered is the front steering angle of the vehicles:

- α_{a_0} for the leader, and α_{d_i} for the followers, with $0 \leq i \leq n-2$.

Frames $(\mathbf{d}_i)$ and $(\mathbf{b}_i)$ have the same origin, but they differ as $(\mathbf{d}_i)$ may rotate due to steering.

In the following, most indices refer to frames $(\mathbf{a})$, $(\mathbf{b})$, $(\mathbf{c})$, or $(\mathbf{d})$. Index i, with $0 \leq i \leq n-1$, represents a particular frame in a module, the inertia matrix $\mathbf{M}_i$ being computed at the origin of this frame.

A posture or power variable that is indexed by a frame index is computed in this frame. In particular, indices $(\cdot)_\parallel$ and $(\cdot)_\perp$ refer respectively to the longitudinal and lateral components - relative to a module - of these variables.

2.2. Kinematic Model

The twist components of the system are given by $\mathbf{T} = \begin{bmatrix} \omega \\ \mathbf{v} \end{bmatrix}$, where ω is the angular velocity, and $\mathbf{v}$, a 2D translation velocity vector.

For the modeling and the selection of vector components, some selection matrices are used:

- $\mathbf{S}_\omega = \begin{bmatrix} 1 & 0 & 0 \end{bmatrix}$, for the selection of angular velocity;

- $\mathbf{S_v} = \begin{bmatrix} 0 & 1 & 0 \\ 0 & 0 & 1 \end{bmatrix}$, for the selection of translation velocity;
- $\mathbf{S_{v_\parallel}} = \begin{bmatrix} 0 & 1 & 0 \end{bmatrix}$, for the selection of longitudinal component of the translation velocity;
- $\mathbf{S_{v_\perp}} = \begin{bmatrix} 0 & 0 & 1 \end{bmatrix}$, for the selection of lateral component of the translation velocity.

Also, the adjoint transformation matrix associated with posture $\mathbf{H}$, which transforms twists from one coordinate frame to another, is given as:

- $\mathbf{Ad_H} = \begin{bmatrix} 1 & \mathbf{O}_{1\times 2} \\ -\mathbf{Jp} & \mathbf{R} \end{bmatrix}$ with $\mathbf{J} = \begin{bmatrix} 0 & -1 \\ 1 & 0 \end{bmatrix}$.

Rather than $\mathbf{Ad_H}$, the following models use the ${}^{\mathbf{y}}\mathbf{Ad_x}$ notation, where $\mathbf{H}$ defines the transformation: frame ($\mathbf{x}$) relative to frame ($\mathbf{y}$). $\mathbf{x}$ and $\mathbf{y}$ can be written $\mathbf{a}_i$, $\mathbf{b}_i$, $\mathbf{c}_i$, $\mathbf{d}_i$ or simply i. When $\mathbf{y}$ is missing, default (i) frame of i^{th} module is considered, when the ($\mathbf{x}$) frame also belongs to the i^{th} module.

Then, the kinematic model corresponds to the following kinematic constraints: the longitudinal velocity is imposed by the leader; the lateral velocity is zero for all wheels; the linear velocity of $i-1$ and i modules is the same at the link point.

Mathematically, these constraints are expressed as:

$$\begin{cases} \mathbf{S}_{v_\parallel}\mathbf{Ad}_{\mathbf{b}_0}^{-1}\mathbf{T}_0 & = & v_0 \\ \mathbf{S}_{v_\perp}\mathbf{Ad}_{\mathbf{a}_0}^{-1}\mathbf{T}_0 & = & 0 \\ \mathbf{S}_{v_\perp}\mathbf{Ad}_{\mathbf{b}_0}^{-1}\mathbf{T}_0 & = & 0 \\ & \dots & \\ \mathbf{S}_{v_\perp}\mathbf{Ad}_{\mathbf{b}_i}^{-1}\mathbf{T}_i & = & 0 \\ \mathbf{S}_v\left({}^i\mathbf{Ad}_{\mathbf{c}_{i-1}}^{-1}\mathbf{T}_i - \mathbf{Ad}_{\mathbf{c}_{i-1}}^{-1}\mathbf{T}_{i-1}\right) & = & 0 \end{cases} \quad (1)$$

By imposing the value v_0, all $\mathbf{T}_i$ twists result from equations (1).

2.3. Dynamic Model

The dynamic model is built in a modular way, considering each module independently as a solid, coupled to the others by dynamic constraints. Wrenches components are given by $\mathbf{W} = \begin{bmatrix} \tau \\ \mathbf{f} \end{bmatrix}$, where τ is a moment and $\mathbf{f}$ a 2D force vector.

As previously, selection matrices are used:

- $\mathbf{S}_\tau = \begin{bmatrix} 1 & 0 & 0 \end{bmatrix}$, for the selection of moment;
- $\mathbf{S_f} = \begin{bmatrix} 0 & 1 & 0 \\ 0 & 0 & 1 \end{bmatrix}$, for the selection of force;
- $\mathbf{S}_{\mathbf{f}_\parallel} = \begin{bmatrix} 0 & 1 & 0 \end{bmatrix}$, for the selection of longitudinal component of the force;
- $\mathbf{S}_{\mathbf{f}_\perp} = \begin{bmatrix} 0 & 0 & 1 \end{bmatrix}$, for the selection of lateral component of the force;

Also, the Lie bracket operation matrix associated with twist $\mathbf{T}$ is considered:

- $\mathbf{ad_T} = \begin{bmatrix} 0 & \mathbf{O}_{1\times 2} \\ -\mathbf{Jv} & \omega\mathbf{J} \end{bmatrix}$

The dynamic vehicle model does not include a longitudinal ground-tire model that is considered perfect. $(\mathbf{a}_0)$ and $(\mathbf{d}_i)$ frames are only controlled by the steering, so they do not generate longitudinal forces or torques. $(\mathbf{b}_i)$ frames can generate longitudinal forces as well as torques. All frames generate lateral forces. Thus, the application of the Newton-Euler equations to the modules

leads to the following equations:

$$\left\{\begin{array}{lcl}
\mathbf{M}_0\dot{\mathbf{T}}_0 & = & \mathbf{ad}^t_{\mathbf{T}_0}\left(\mathbf{M}_0\mathbf{T}_0\right) + \mathbf{Ad}^{-t}_{\mathbf{a}_0}\mathbf{S}^t_{\mathbf{f}_\perp}\mathbf{f}_{\mathbf{a}_{0\perp}} + \mathbf{Ad}^{-t}_{\mathbf{b}_0}\mathbf{S}^t_{\mathbf{f}_\perp}\mathbf{f}_{\mathbf{b}_{0\perp}} \\
 & & +\mathbf{Ad}^{-t}_{\mathbf{d}_0}\mathbf{S}^t_{\mathbf{f}_\perp}\mathbf{f}_{\mathbf{d}_{0\perp}} + \mathbf{Ad}^{-t}_{\mathbf{b}_0}\left[\mathbf{S}^t_{\mathbf{f}_\parallel}\mathbf{f}_{\mathbf{b}_{0\parallel}} + \mathbf{S}^t_\tau\tau_{\mathbf{b}_0}\right] \\
 & & +\mathbf{Ad}^{-t}_{\mathbf{c}_0}\mathbf{W}_{\mathbf{c}_0} \\
 & \cdots & \\
\mathbf{M}_i\dot{\mathbf{T}}_i & = & \mathbf{ad}^t_{\mathbf{T}_i}\left(\mathbf{M}_i\mathbf{T}_i\right) + \mathbf{Ad}^{-t}_{\mathbf{b}_i}\mathbf{S}^t_{\mathbf{f}_\perp}\mathbf{f}_{\mathbf{b}_{i\perp}} + \mathbf{Ad}^{-t}_{\mathbf{d}_i}\mathbf{S}^t_{\mathbf{f}_\perp}\mathbf{f}_{\mathbf{d}_{i\perp}} \\
 & & +\mathbf{Ad}^{-t}_{\mathbf{b}_i}\left[\mathbf{S}^t_{\mathbf{f}_\parallel}\mathbf{f}_{\mathbf{b}_{i\parallel}} + \mathbf{S}^t_\tau\tau_{\mathbf{b}_i}\right] + \mathbf{Ad}^{-t}_{\mathbf{a}_i}\mathbf{S}^t_\tau\tau_{\mathbf{a}_i} \\
 & & +\mathbf{Ad}^{-t}_{\mathbf{c}_i}\mathbf{W}_{\mathbf{c}_i} + \mathbf{Ad}^{-t}_{\mathbf{a}_i}\mathbf{S}^t_{\mathbf{f}}\mathbf{f}_{\mathbf{a}_i} \\
 & \cdots & \\
\mathbf{M}_{n-1}\dot{\mathbf{T}}_{n-1} & = & \mathbf{ad}^t_{\mathbf{T}_{n-1}}\left(\mathbf{M}_{n-1}\mathbf{T}_{n-1}\right) + \mathbf{Ad}^{-t}_{\mathbf{b}_{n-1}}\mathbf{S}^t_{\mathbf{f}_\perp}\mathbf{f}_{\mathbf{b}_{n-1\perp}} \\
 & & +\mathbf{Ad}^{-t}_{\mathbf{b}_{n-1}}\left[\mathbf{S}^t_{\mathbf{f}_\parallel}\mathbf{f}_{\mathbf{b}_{n-1\parallel}} + \mathbf{S}^t_\tau\tau_{\mathbf{b}_{n-1}}\right] + \mathbf{Ad}^{-t}_{\mathbf{a}_{n-1}}\mathbf{S}^t_\tau\tau_{\mathbf{a}_{n-1}} \\
 & & +\mathbf{Ad}^{-t}_{\mathbf{a}_{n-1}}\mathbf{S}^t_{\mathbf{f}}\mathbf{f}_{\mathbf{a}_{n-1}}
\end{array}\right. \tag{2}$$

For the lateral ground-tire dynamics, a first-order model was chosen. This model is described in [13], and is close to a slightly more complex formulation known as **TMEASY** described in [14].

For $\mathbf{x} = \mathbf{a}_0$, $\mathbf{b}_i$ with $0 \leq i \leq n-1$, or $\mathbf{d}_j$ with $0 \leq j \leq n-2$:

$$\dot{\mathbf{f}}_{\mathbf{x}_\perp} = -\kappa\left(\mathbf{S}_{\mathbf{v}_\parallel}\mathbf{Ad}^{-1}_{\mathbf{x}}\mathbf{T}\right)\mathbf{S}_{\mathbf{v}_\perp}\mathbf{Ad}^{-1}_{\mathbf{x}}\mathbf{T} - \omega\left(\mathbf{S}_{\mathbf{v}_\parallel}\mathbf{Ad}^{-1}_{\mathbf{x}}\mathbf{T}\right)\mathbf{f}_{\mathbf{x}_\perp} \tag{3}$$

where:

- $\omega\left(\cdot\right) = \frac{c_y|\cdot|}{k_d + d_y|\cdot|}$
- $\kappa\left(\cdot\right) = \frac{c_y k_d}{k_d + d_y|\cdot|}$

with k_d, c_y, and d_y being respectively the drift stiffness, the tire stiffness and damping characteristics.

Then, constraints eliminate $\mathbf{f_a}$ and $\mathbf{W_c}$ terms.

Kinematic constraints at vehicles coupling point are:

$$\text{For } 1 \leq i \leq n-1 : \mathbf{S}_v\left({}^{i-1}\mathbf{Ad}^{-1}_{\mathbf{a}_i}\mathbf{T}_{i-1} - \mathbf{Ad}^{-1}_{\mathbf{a}_i}\mathbf{T}_i\right) = 0$$

Kinematic constraints must be expressed in terms of accelerations in order to

be used with dynamic equations. They are then rewritten as follows:

$$\text{For } 1 \leq i \leq n-1 : \mathbf{S}_v \left({}^{i-1}\mathbf{Ad}_{\mathbf{a}_i}^{-1} \dot{\mathbf{T}}_{i-1} - \mathbf{Ad}_{\mathbf{a}_i}^{-1} \dot{\mathbf{T}}_i \right) = \mathbf{S}_v \mathbf{Ad}_{\mathbf{a}_i}^{-1} \mathbf{ad}_i{}^i \mathbf{Ad}_{i-1} \mathbf{T}_{i-1} \tag{4}$$

Similarly, the dynamic constraints at the coupling point of the vehicles are:

$$\text{For } 1 \leq i \leq n-1 : 0 = \mathbf{S}_\tau^t \tau_{\mathbf{a}_i} + {}^{\mathbf{a}_i}\mathbf{Ad}_{\mathbf{c}_{i-1}}^{-t} \mathbf{W}_{\mathbf{c}_{i-1}} + \mathbf{S}_{\mathbf{f}}^t \mathbf{f}_{\mathbf{a}_i} \tag{5}$$

2.4. Linearized Dynamic Model

Control algorithms computed in the following are based on a linearized model. It is therefore proposed here to linearize the previous dynamic model. Linearization of dynamic equations (2) gives:

$$\left\{ \begin{array}{lcl}
\mathbf{M}_0 \delta \dot{\mathbf{T}}_0 & = & \left(\mathbf{ad}_{\mathbf{T}_0}^t \mathbf{M}_0 - \mathbf{ad}_{\mathbf{M}_0 \mathbf{T}_0}^w \right) \delta \mathbf{T}_0 + \mathbf{Ad}_{\mathbf{a}_0}^{-t} \mathbf{S}_{\mathbf{f}_\perp}^t \delta \mathbf{f}_{\mathbf{a}_{0\perp}} \\
& & + \mathbf{Ad}_{\mathbf{b}_0}^{-t} \mathbf{S}_{\mathbf{f}_\perp}^t \delta \mathbf{f}_{\mathbf{b}_{0\perp}} + \mathbf{Ad}_{\mathbf{d}_0}^{-t} \mathbf{S}_{\mathbf{f}_\perp}^t \delta \mathbf{f}_{\mathbf{d}_{0\perp}} \\
& & + \mathbf{Ad}_{\mathbf{a}_0}^{-t} \mathbf{ad}_{\mathbf{S}_{\mathbf{f}_\perp}^t \mathbf{f}_{\mathbf{a}_{0\perp}}}^w \mathbf{S}_\omega^t \delta \alpha_{\mathbf{a}_0} + \mathbf{Ad}_{\mathbf{d}_0}^{-t} \mathbf{ad}_{\mathbf{S}_{\mathbf{f}_\perp}^t \mathbf{f}_{\mathbf{d}_{0\perp}}}^w \mathbf{S}_\omega^t \delta \alpha_{\mathbf{d}_0} \\
& & + \mathbf{Ad}_{\mathbf{b}_0}^{-t} \left[\mathbf{S}_{\mathbf{f}_\parallel}^t \delta \mathbf{f}_{\mathbf{b}_{0\parallel}} + \mathbf{S}_\tau^t \delta \tau_{\mathbf{b}_0} \right] + \mathbf{Ad}_{\mathbf{c}_0}^{-t} \delta \mathbf{W}_{\mathbf{c}_0} \\
& \cdots & \\
\mathbf{M}_i \delta \dot{\mathbf{T}}_i & = & \left(\mathbf{ad}_{\mathbf{T}_i}^t \mathbf{M}_i - \mathbf{ad}_{\mathbf{M}_i \mathbf{T}_i}^w \right) \delta \mathbf{T}_i + \mathbf{Ad}_{\mathbf{b}_i}^{-t} \mathbf{S}_{\mathbf{f}_\perp}^t \delta \mathbf{f}_{\mathbf{b}_{i\perp}} \\
& & + \mathbf{Ad}_{\mathbf{d}_i}^{-t} \mathbf{S}_{\mathbf{f}_\perp}^t \delta \mathbf{f}_{\mathbf{d}_{i\perp}} + \mathbf{Ad}_{\mathbf{d}_i}^{-t} \mathbf{ad}_{\mathbf{S}_{\mathbf{f}_\perp}^t \mathbf{f}_{\mathbf{d}_{i\perp}}}^w \mathbf{S}_\omega^t \delta \alpha_{\mathbf{d}_i} \\
& & + \mathbf{Ad}_{\mathbf{b}_i}^{-t} \left[\mathbf{S}_{\mathbf{f}_\parallel}^t \delta \mathbf{f}_{\mathbf{b}_{i\parallel}} + \mathbf{S}_\tau^t \delta \tau_{\mathbf{b}_i} \right] + \mathbf{Ad}_{\mathbf{a}_i}^{-t} \mathbf{S}_\tau^t \delta \tau_{\mathbf{a}_i} \\
& & + \mathbf{Ad}_{\mathbf{c}_i}^{-t} \delta \mathbf{W}_{\mathbf{c}_i} + \mathbf{Ad}_{\mathbf{a}_i}^{-t} \mathbf{S}_{\mathbf{f}}^t \delta \mathbf{f}_{\mathbf{a}_i} \\
& \cdots & \\
\mathbf{M}_{n-1} \delta \dot{\mathbf{T}}_{n-1} & = & \left(\mathbf{ad}_{\mathbf{T}_{n-1}}^t \mathbf{M}_{n-1} - \mathbf{ad}_{\mathbf{M}_{n-1} \mathbf{T}_{n-1}}^w \right) \delta \mathbf{T}_{n-1} + \mathbf{Ad}_{\mathbf{b}_{n-1}}^{-t} \mathbf{S}_{\mathbf{f}_\perp}^t \delta \mathbf{f}_{\mathbf{b}_{n-1\perp}} \\
& & + \mathbf{Ad}_{\mathbf{b}_{n-1}}^{-t} \left[\mathbf{S}_{\mathbf{f}_\parallel}^t \delta \mathbf{f}_{\mathbf{b}_{n-1\parallel}} + \mathbf{S}_\tau^t \delta \tau_{\mathbf{b}_{n-1}} \right] + \mathbf{Ad}_{\mathbf{a}_{n-1}}^{-t} \mathbf{S}_\tau^t \delta \tau_{\mathbf{a}_{n-1}} \\
& & + \mathbf{Ad}_{\mathbf{a}_{n-1}}^{-t} \mathbf{S}_{\mathbf{f}}^t \delta \mathbf{f}_{\mathbf{a}_{n-1}}
\end{array} \right. \tag{6}$$

Linearization of the lateral dynamic ground-tire model (3) gives:

For $\mathbf{x} = \mathbf{b}_i$ with $0 \leq i \leq n-1$:

$$\begin{array}{rcl}
\delta \dot{\mathbf{f}}_{\mathbf{x}_\perp} & = & - \left[\left(d\omega \left(\mathbf{T} \right) \mathbf{f}_{\mathbf{x}_\perp} + d\kappa \left(\mathbf{T} \right) \mathbf{S}_{\mathbf{v}_\perp} \mathbf{Ad}_{\mathbf{x}}^{-1} \mathbf{T} \right) \mathbf{S}_{\mathbf{v}_\parallel} \right. \\
& & \left. + \kappa \left(\mathbf{T} \right) \mathbf{S}_{\mathbf{v}_\perp} \right] \mathbf{Ad}_{\mathbf{x}}^{-1} \delta \mathbf{T} - \omega \left(\mathbf{T} \right) \delta \mathbf{f}_{\mathbf{x}_\perp}
\end{array} \tag{7}$$

For $\mathbf{x} = \mathbf{a}_0$, or $\mathbf{d}_j$ with $0 \leq j \leq n-2$:

$$\begin{aligned}\delta\dot{\mathbf{f}}_{\mathbf{x}_\perp} &= -\left[\left(d\omega\left(\mathbf{T}\right)\mathbf{f}_{\mathbf{x}_\perp} + d\kappa\left(\mathbf{T}\right)\mathbf{S}_{\mathbf{v}_\perp}\mathbf{Ad}_{\mathbf{x}}^{-1}\mathbf{T}\right)\mathbf{S}_{\mathbf{v}_\parallel}\right. \\ &\quad \left.+\kappa\left(\mathbf{T}\right)\mathbf{S}_{\mathbf{v}_\perp}\right]\mathbf{Ad}_{\mathbf{x}}^{-1}\delta\mathbf{T} - \omega\left(\mathbf{T}\right)\delta\mathbf{f}_{\mathbf{x}_\perp} - \left[\left(d\omega\left(\mathbf{T}\right)\mathbf{f}_{\mathbf{x}_\perp}\right.\right. \\ &\quad \left.\left.+d\kappa\left(\mathbf{T}\right)\mathbf{S}_{\mathbf{v}_\perp}\mathbf{Ad}_{\mathbf{x}}^{-1}\mathbf{T}\right)\mathbf{S}_{\mathbf{v}_\parallel} + \kappa\left(\mathbf{T}\right)\mathbf{S}_{\mathbf{v}_\perp}\right]\mathbf{Ad}_{\mathbf{x}}^{-1}\mathbf{ad}_{\mathbf{T}}\mathbf{Ad}_{\mathbf{x}}\mathbf{S}_\omega^t\delta\alpha_{\mathbf{x}}\end{aligned} \tag{8}$$

Linearized constraints eliminate $\delta\mathbf{f}_{\mathbf{a}}$ and $\delta\mathbf{W}_{\mathbf{c}}$ terms.

Linearization of kinematic constraints equation (4) gives:

For $1 \leq i \leq n-1$:

$$\begin{aligned}&\mathbf{S}_v\left({}^{i-1}\mathbf{Ad}_{\mathbf{a}_i}^{-1}\delta\dot{\mathbf{T}}_{i-1} - \mathbf{Ad}_{\mathbf{a}_i}^{-1}\delta\dot{\mathbf{T}}_i\right) = \\ &-\mathbf{S}_v\mathbf{Ad}_{\mathbf{a}_i}^{-1}\left({}^i\mathbf{Ad}_{i-1}\mathbf{ad}_{\dot{\mathbf{T}}_{i-1}} - \mathbf{ad}_i{}^i\mathbf{Ad}_{i-1}\mathbf{ad}_{i-1}\right){}^{i-1}\mathbf{Ad}_{\mathbf{a}_i}\mathbf{S}_\omega^t\delta\theta_{i-1,i} \\ &+\mathbf{S}_v\left(\mathbf{Ad}_{\mathbf{a}_i}^{-1}\mathbf{ad}_i{}^i\mathbf{Ad}_{i-1}\delta\mathbf{T}_{i-1} - {}^{i-1}\mathbf{Ad}_{\mathbf{a}_i}^{-1}\mathbf{ad}_{i-1}{}^i\mathbf{Ad}_{i-1}^{-1}\delta\mathbf{T}_i\right)\end{aligned} \tag{9}$$

Linearization of dynamic constraints equation (5) gives:

For $1 \leq i \leq n-1$:

$$0 = -{}^{\mathbf{a}_i}\mathbf{Ad}_{\mathbf{c}_{i-1}}^{-t}\mathbf{ad}_{\mathbf{W}_{\mathbf{c}_{i-1}}}^w\mathbf{S}_\omega^t\delta\theta_{i-1,i} + \mathbf{S}_\tau^t\delta\tau_{\mathbf{a}_i} + {}^{\mathbf{a}_i}\mathbf{Ad}_{\mathbf{c}_{i-1}}^{-t}\delta\mathbf{W}_{\mathbf{c}_{i-1}} + \mathbf{S}_{\mathbf{f}}^t\delta\mathbf{f}_{\mathbf{a}_i} \tag{10}$$

For a more compact writing of the equations, the following term which is associated with the wrench $\mathbf{W}$ is used in the linearized equations above:

$\mathbf{ad}_{\mathbf{W}}^w = \begin{bmatrix} 0 & \mathbf{f}^t\mathbf{J} \\ \mathbf{Jf} & \mathbf{O}_{2\times 2} \end{bmatrix}$.

3. Stabilization control

3.1. The reference

A natural choice of control reference would be a road-train following a desired trajectory with an ideal kinematic model (rolling without slipping). But the trajectories are not known *a priori*, especially in the event of an emergency maneuver. One way to solve this difficulty is to link the first vehicle of the real road-train system to its kinematic avatar. The only drawback of this solution is that in the event of high instability, the first module of the real road-train may oscillate, and cause its kinematic avatar to oscillate in the same way. Thus, the

control must be efficient enough to react before such oscillations or to cancel them quickly enough.

The available information is the current state of the real system and the driver's inputs. Depending on the driver's steering and propulsion inputs, the pose with the reference kinematics may deviate from that of the real system. It is therefore necessary to adjust the kinematic reference pose to that of the real system. In practice, the position and orientation of the first vehicle of the reference road train are continuously updated with a conventional extended Kalman filter [15] that takes into account the yaw angle measurement provided by a gyrometer sensor.

To establish the configuration of the reference road-train, it is sufficient to calculate the relative orientations and rotational speeds of each of the following vehicles in relation to their predecessor. They are determined from the kinematic model, knowing the steering and speed of the first vehicle.

Control is based on a comparison between reference and actual system configuration. More precisely, control inputs consist of the following *Output Error Vector*:

$$\mathbf{X} = \begin{bmatrix} \mathbf{h}_0 - \mathbf{h}_{0_{ref}} \\ \theta_{0,1} - \theta_{0,1_{ref}} \\ \vdots \\ \theta_{i-1,i} - \theta_{i-1,i_{ref}} \\ \vdots \\ \theta_{n-2,n-1} - \theta_{n-2,n-1_{ref}} \\ \dot{\mathbf{h}}_0 - \dot{\mathbf{h}}_{0_{ref}} \\ \dot{\theta}_{0,1} - \dot{\theta}_{0,1_{ref}} \\ \vdots \\ \dot{\theta}_{i-1,i} - \dot{\theta}_{i-1,i_{ref}} \\ \vdots \\ \dot{\theta}_{n-2,n-1} - \dot{\theta}_{n-2,n-1_{ref}} \end{bmatrix} \tag{11}$$

where the index $()_{ref}$ stands for *reference*.

3.2. Propulsion control

All vehicles participate in the propulsion by minimizing inter-vehicle forces. Dynamic equations (2) are used for the computation of the anticipation wrenches. In these equations, coupling forces are zero and the steering of the towed vehicles is not taken into account. So, for $1 \leq i \leq n-1$: $\mathbf{W}_{\mathbf{a}_i} = \mathbf{0}_{3\times 1}$ and for $0 \leq i \leq n-2$: $\mathbf{W}_{\mathbf{c}_i} = \mathbf{0}_{3\times 1}$ and $\mathbf{f}_{\mathbf{d}_{i\perp}} = 0$. Twists and accelerations are computed with kinematic model (1) from the driver's speed input v_0 and its derivative. It is then possible to compute the actuating wrenches (wheel motors and brakes) for each module. For the Leader module, the distribution of lateral forces between the front and rear trains must be chosen.

To avoid high drive wheel speeds in the event of slippage or high force values due to model errors, anticipation wrenches are combined with complementary wrenches resulting from proportional control of the wheel speeds to speed setpoints of the reference model. These control coefficients are low enough not to interfere too much with anticipation.

3.3. System control inputs

Three different control inputs are considered:

- **Steer control**: stabilization is only controlled by the front-axle steering of each vehicle (($\mathbf{a}_0$) and ($\mathbf{d}_i$) frames - $0 \leq i \leq n-2$ - in Fig. 1 and 2);
- **Drive control**: stabilization is only controlled by engines and brakes on the rear axle of each vehicle (($\mathbf{b}_i$) frames - $0 \leq i \leq n-1$ - in Fig. 1 to 3).
- **Damper control**: stabilization is only controlled by joint dampers. These dampers are fitted to all vehicles. In Fig. 1 to 3, joint dampers affect the rotation of frames ($\mathbf{c}_{i-1}$) relative to frames ($\mathbf{a}_i$) - $1 \leq i \leq n-1$.

3.4. Control structure and tuning

Even if a control based on localization could make sense, with a control of each module that depends only on its own state, a dependence on previous and following modules cannot be excluded. A global synthesis approach was therefore chosen.

Synthesis based on a linearized model is studied: **LQR** - Linear Quadratic Regulator. Due to variability of environmental conditions, especially ground-tire characteristics, synthesis approaches of moderate complexity are preferable to investigate robustness issues.

With the three control inputs described above, and on the basis of the previous linearized dynamic model (6), the elimination of constraints (9)-(10) leads to the following new state equation.

$$\mathbf{E}\dot{\mathbf{x}} = \mathbf{F}\mathbf{x} + \mathbf{G}_s\mathbf{u}_s + \mathbf{G}_m\mathbf{u}_m + \mathbf{G}_d\mathbf{u}_d + \mathbf{H}\mathbf{v} \tag{12}$$

with:

- $\mathbf{x} = \begin{bmatrix} \left[\mathbf{h}_0^t - \mathbf{h}_{0_{ref}}^t, \theta_{0,1} - \theta_{0,1_{ref}}, \cdots, \theta_{i-1,i} - \theta_{i-1,i_{ref}}, \cdots, \theta_{n-2,n-1} - \theta_{n-2,n-1_{ref}}\right]^t \\ \left[\mathbf{T}_0^t - \mathbf{T}_{0_{ref}}^t, \cdots, \mathbf{T}_i^t - \mathbf{T}_{i_{ref}}^t, \cdots, \mathbf{T}_{n-1}^t - \mathbf{T}_{n-1_{ref}}^t\right]^t \\ \left[\delta f_{\mathbf{a}_0\perp}, \delta f_{\mathbf{b}_0\perp}, \cdots, \delta f_{\mathbf{b}_i\perp}, \cdots, \delta f_{\mathbf{b}_{n-1}\perp}, \delta f_{\mathbf{d}_0\perp}, \cdots, \delta f_{\mathbf{d}_i\perp}, \cdots, \delta f_{\mathbf{d}_{n-2}\perp}\right]^t \end{bmatrix}$ the state;
- $\mathbf{u}_s = \left[\delta\alpha_{\mathbf{a}_0}, \delta\alpha_{\mathbf{d}_0}, \cdots, \delta\alpha_{\mathbf{d}_i}, \cdots, \delta\alpha_{\mathbf{d}_{n-2}}\right]^t$ the Steer Control input;
- $\mathbf{u}_m = \left[\delta f_{\mathbf{b}_{0\parallel}}, \cdots, \delta f_{\mathbf{b}_{i\parallel}}, \cdots, \delta f_{\mathbf{b}_{n-1\parallel}}, \delta\tau_{\mathbf{b}_0}, \cdots, \delta\tau_{\mathbf{b}_i}, \cdots, \delta\tau_{\mathbf{b}_{n-1}}\right]^t$ the Drive Control input;
- $\mathbf{u}_d = \left[\delta\tau_{\mathbf{a}_1}, \cdots, \delta\tau_{\mathbf{a}_i}, \cdots, \delta\tau_{\mathbf{a}_{n-1}}\right]^t$ the Damper Control input;
- $\mathbf{v} = \left[\delta\mathbf{W}_{\mathbf{c}_0}^t, \cdots, \delta\mathbf{W}_{\mathbf{c}_i}^t, \cdots, \delta\mathbf{W}_{\mathbf{c}_{n-2}}^t, \delta\mathbf{f}_{\mathbf{a}_1}^t, \cdots, \delta\mathbf{f}_{\mathbf{a}_i}^t, \cdots, \delta\mathbf{f}_{\mathbf{a}_{n-1}}^t\right]^t$ the vector of linked wrenches that can be deleted by introducing kinematic constraints.

Then, considering that the lateral forces have a fast dynamics with an establishment time fast enough to be neglected, the following vector is set to zero.

$$\delta\dot{\mathbf{f}}_{\perp} = \left[\delta\dot{f}_{\mathbf{a}_{0_{\perp}}}, \delta\dot{f}_{\mathbf{b}_{0_{\perp}}}, \cdots, \delta\dot{f}_{\mathbf{b}_{i_{\perp}}}, \cdots, \delta\dot{f}_{\mathbf{b}_{n-1_{\perp}}}, \delta\dot{f}_{\mathbf{d}_{0_{\perp}}}, \cdots, \delta\dot{f}_{\mathbf{d}_{i_{\perp}}}, \cdots, \delta\dot{f}_{\mathbf{d}_{n-2_{\perp}}}\right]^t$$

Thus, left side of equations (7)-(8) is zero, and they are therefore used as new constraint equations where lateral forces are new constrained variables. As a result, the corresponding state variables below are linked.

$$\delta\mathbf{f}_{\perp} = \left[\delta f_{\mathbf{a}_{0_{\perp}}}, \delta f_{\mathbf{b}_{0_{\perp}}}, \cdots, \delta f_{\mathbf{b}_{i_{\perp}}}, \cdots, \delta f_{\mathbf{b}_{n-1_{\perp}}}, \delta f_{\mathbf{d}_{0_{\perp}}}, \cdots, \delta f_{\mathbf{d}_{i_{\perp}}}, \cdots, \delta f_{\mathbf{d}_{n-2_{\perp}}}\right]^t$$

Simplification of the previous linearized model (12) by adding them to vector $\mathbf{v}$ leads to the new state equation below.

$$\mathbf{E}_{\sigma}\dot{\mathbf{x}}_{\sigma} = \mathbf{F}_{\sigma}\mathbf{x}_{\sigma} + \mathbf{G}_s\mathbf{u}_s + \mathbf{G}_m\mathbf{u}_m + \mathbf{G}_d\mathbf{u}_d + \mathbf{H}_{\sigma}\mathbf{v}_{\sigma} \tag{13}$$

with:

- $\mathbf{x}_{\sigma} = \begin{bmatrix} \left[\mathbf{h}_0^t - \mathbf{h}_{0_{ref}}^t, \theta_{0,1} - \theta_{0,1_{ref}}, \cdots, \theta_{i-1,i} - \theta_{i-1,i_{ref}}, \cdots, \theta_{n-2,n-1} - \theta_{n-2,n-1_{ref}}\right]^t \\ \left[\mathbf{T}_0^t - \mathbf{T}_{0_{ref}}^t, \cdots, \mathbf{T}_i^t - \mathbf{T}_{i_{ref}}^t, \cdots, \mathbf{T}_{n-1}^t - \mathbf{T}_{n-1_{ref}}^t\right]^t \end{bmatrix}$;
- $\mathbf{v}_{\sigma} = [\delta\mathbf{f}_{\perp}^t, \mathbf{v}^t]^t$;
- $\mathbf{E}_{\sigma}$ is computed from matrix $\mathbf{E}$ where columns corresponding to vector $\mathbf{f}_{\perp}$ are removed ($\mathbf{E} = [\mathbf{E}_{\sigma}, \mathbf{E}_{\mathbf{f}_{\perp}}]$);
- $\mathbf{F}_{\sigma}$ is computed from matrix $\mathbf{F}$ where columns corresponding to vector $\mathbf{f}_{\perp}$ are removed ($\mathbf{F} = [\mathbf{F}_{\sigma}, \mathbf{F}_{\mathbf{f}_{\perp}}]$);
- $\mathbf{H}_{\sigma} = [\mathbf{F}_{\mathbf{f}_{\perp}}, \mathbf{H}]$.

An implicit discretization step, by augmenting the state with constraint variables, gives the following state equation.

$$\mathbf{E}_{\delta}\begin{bmatrix} \mathbf{x}_{\sigma_{k+1}} \\ \mathbf{v}_{\sigma_{k+1}} \end{bmatrix} = \mathbf{E}_{\sigma}\mathbf{x}_{\sigma\,k} + dt\mathbf{G}_z\mathbf{u}_z \tag{14}$$

with:

- dt the sampling time;
- $\mathbf{E}_\delta = [\mathbf{E}_\sigma - dt\mathbf{F}_\sigma; -dt\mathbf{H}_\sigma]$;
- indice z is equal to s, m, or d depending on the controller to be considered.

$\mathbf{E}_\delta$ being invertible, equation 14 can be written as follows.

$$\begin{bmatrix} \mathbf{x}_{\sigma_{k+1}} \\ \mathbf{v}_{\sigma_{k+1}} \end{bmatrix} = \mathbf{E}_\delta^{-1}\mathbf{E}_\sigma \mathbf{x}_{\sigma\, k} + dt\mathbf{E}_\delta^{-1}\mathbf{G}_z\mathbf{u}_z$$

Then, submatrix $\mathbf{E}_{\delta,\rho}^{-1}$ is the extraction of r first lines of $\mathbf{E}_\delta^{-1}$, with $r = \dim(\mathbf{x}_\sigma)$, in order to select only the upper part of the equation.

$$\mathbf{x}_{\sigma_{k+1}} = \mathbf{E}_{\delta,\rho}^{-1}\mathbf{E}_\sigma \mathbf{x}_{\sigma\, k} + dt\mathbf{E}_{\delta,\rho}^{-1}\mathbf{G}_z\mathbf{u}_z$$

Reduction of this model to a model with only independant state variables is done by considering a transformation matrix $\mathbf{P}$ verifying equality below.

$$\begin{bmatrix} \mathbf{x}_\rho \\ \mathbf{0}_{2(n-1)\times 1} \end{bmatrix} = \begin{bmatrix} \mathbf{h}_0 - \mathbf{h}_{0_{ref}} \\ \theta_{0,1} - \theta_{0,1_{ref}} \\ \vdots \\ \theta_{i-1,i} - \theta_{i-1,i_{ref}} \\ \vdots \\ \theta_{n-2,n-1} - \theta_{n-2,n-1_{ref}} \\ \dot{\mathbf{h}}_0 - \dot{\mathbf{h}}_{0_{ref}} \\ \dot{\theta}_{0,1} - \dot{\theta}_{0,1_{ref}} \\ \vdots \\ \dot{\theta}_{i-1,i} - \dot{\theta}_{i-1,i_{ref}} \\ \vdots \\ \dot{\theta}_{n-2,n-1} - \dot{\theta}_{n-2,n-1_{ref}} \\ \mathbf{0}_{2(n-1)\times 1} \end{bmatrix} = \mathbf{P} \begin{bmatrix} \mathbf{h}_0 - \mathbf{h}_{0_{ref}} \\ \theta_{0,1} - \theta_{0,1_{ref}} \\ \vdots \\ \theta_{i-1,i} - \theta_{i-1,i_{ref}} \\ \vdots \\ \theta_{n-2,n-1} - \theta_{n-2,n-1_{ref}} \\ \mathbf{T}_0 - \mathbf{T}_{0_{ref}} \\ \vdots \\ \mathbf{T}_i - \mathbf{T}_{i_{ref}} \\ \vdots \\ \mathbf{T}_{n-1} - \mathbf{T}_{n-1_{ref}} \end{bmatrix} = \mathbf{P}\mathbf{x}_\sigma$$

Last lines of this vector ($\mathbf{0}_{2(n-1)\times 1}$) correspond to kinematic constraints. Matrix $\mathbf{P}$ is invertible and its inverse is denoted $\mathbf{P}^{-1}$. It is possible to extract sub-

matrices $\mathbf{P}_\rho$ and $\mathbf{P}_\rho^{-1}$ from respectively $\mathbf{P}$ and $\mathbf{P}^{-1}$ so that:

$$\begin{cases} \mathbf{P}_\rho \mathbf{x}_\sigma &= \mathbf{x}_\rho \\ \mathbf{P}_\rho^{-1} \mathbf{x}_\rho &= \mathbf{x}_\sigma \end{cases}$$

Note that $\mathbf{P}_\rho^{-1}$ is not the inverse of $\mathbf{P}_\rho$.

Finally, the discretized state equation is as follows:

$$\mathbf{x}_{\rho k+1} = \mathbf{P}_\rho \mathbf{E}_{\delta,\rho}^{-1} \mathbf{E}_\sigma \mathbf{P}_\rho^{-1} \mathbf{x}_{\rho k} + dt \mathbf{P}_\rho \mathbf{E}_{\delta,\rho}^{-1} \mathbf{G}_z \mathbf{u}_z \tag{15}$$

In equation 15, state matrix $\mathbf{A}$ and gain matrix $\mathbf{B}$ are given by:

- $\mathbf{A} = \mathbf{P}_\rho \mathbf{E}_{\delta,\rho}^{-1} \mathbf{E}_\sigma \mathbf{P}_\rho^{-1}$
- $\mathbf{B} = dt \mathbf{P}_\rho \mathbf{E}_{\delta,\rho}^{-1} \mathbf{G}_z$

Then, the following control input is applied [16]:

$$\mathbf{u}_{z_k} = -\mathbf{K}_z \mathbf{x}_{\rho_k} \tag{16}$$

with $\mathbf{K}_z = \left(\mathbf{B}^t \mathbf{P} \mathbf{B} + \mathbf{R}_z\right)^{-1} \mathbf{B}^t \mathbf{P} \mathbf{A}$ the LQR discrete gain computed from $\mathbf{P}$, a solution of the discrete Riccati equation stabilizing the system, written as

$$\mathbf{A}^t \mathbf{P} \mathbf{A} + \mathbf{Q}_z - \mathbf{A}^t \mathbf{P} \mathbf{B} \left(\mathbf{B}^t \mathbf{P} \mathbf{B} + \mathbf{R}_z\right)^{-1} \mathbf{B}^t \mathbf{P} \mathbf{A} = \mathbf{P}$$

State $\mathbf{Q}_z$ and control input $\mathbf{R}_z$ coefficient matrices are diagonal matrices defining the cost to be minimized: $\mathbf{x}_{\rho_k}^t \mathbf{Q}_z \mathbf{x}_{\rho_k} + \mathbf{u}_{z_k}^t \mathbf{R}_z \mathbf{u}_{z_k}$. $\mathbf{Q}_z$ parameters corresponding to θ_0, $\theta_{i-1,i}$ and their derivatives are set to the same values as $\mathbf{R}_z$ parameters. Other $\mathbf{Q}_z$ parameters corresponding to the position and its derivative are less relevant for the road-train stabilization, and therefore can be set at a lower value.

Then, gain $\mathbf{K}_z$ is computed offline for each control input and for a set of possible values of the first vehicle longitudinal velocity v_0. If the current measured speed is different from those used to compute the gain, an interpolation is performed using the closest lower and upper speeds. Values of $\mathbf{K}_z$ are validated by analyzing eigenvalues of the closed-loop system $\mathbf{A} - \mathbf{B}\mathbf{K}_z$. Eigenvalues must be lower

than 1 for the error state vector to converge to zero, but also large enough to prevent instabilities that may be due to actuator delays or establishment time that was neglected in equation (13).

4. Road-train simulator

A vehicle road-train illustrated in Fig. 4 was modelled in 3D in **MSC ADAMS™** environment (see [17]).

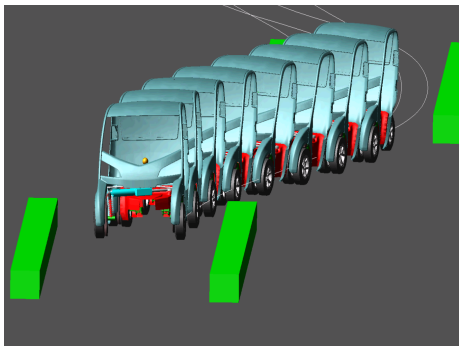

Figure 4: Eight vehicle road-train

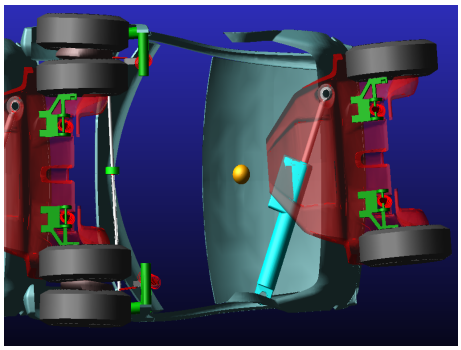

Figure 5: Bottom view of the last coupled vehicle

Each vehicle consists of about 20 rigid parts connected together by joints and actuators or by linear-nonlinear force-torque elements (see Fig. 5). The front wheel axis of each towed vehicle is aligned with the rear wheel axis of the front vehicle to which it is coupled. The damping of its central articulation, illustrated by a yellow ball in Fig. 5, is then regulated by a damper, represented in cyan to the right of this joint.

- Each rigid part is characterized by its connection points for geometry, its mass, inertia and center of mass for dynamics, and an envelope, useful only for graphic purposes;
- Joints between parts have been chosen among different possibilities (Translational, Revolute, Hooke, Spherical) according to the real system and in order to avoid free movements.

Different force-torque elements are added to joints. In particular, a realistic Pacejka 2002 tire model (PAC2002) is implemented (see [18]), its parameters being fully adapted by the real vehicle's tire supplier.

4.1. Force-Torque elements

4.1.1. Torque for Anti-Roll bar

Anti-roll stiffness is modelled by a linear torque stiffness between symmetrical suspension arms.

4.1.2. Force for linear actuator (damper) of central joint

This resistive force is non-linear, characterized by two parameters (see Fig. 6):

- A maximum step force f_0 acting as dry friction, which is controlled;
- A slope value α corresponding to a viscous friction, which depends on the damper design and is not controlled.

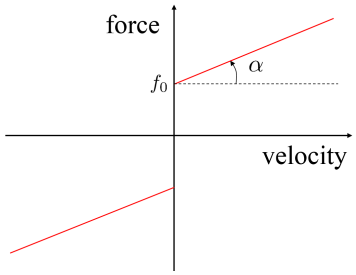

Figure 6: Damper characteristics

4.1.3. Visco-elastic force for suspensions

Suspensions are modelled by standard spring damper elements.

4.1.4. Bushings for coupling devices

In road-train configuration, vehicles are linked together by coupling devices. As infinitely rigid coupling is neither mechanically feasible nor desirable, **bushing** are placed at the interface between each coupling device and the chassis (front or rear).

4.1.5. Wheels torque control

Each wheel torque may be controlled. For simulations presented hereunder, only rear wheel torque is controlled by motors and brakes.

4.1.6. Steering

The steering rack position is controlled by a proportional derivative controller, internal to the simulator, which is following a desired rack position as input.

4.2. Co-simulation

Vehicle control algorithms are implemented in an external $\mathbf{C++}$ program that is interfaced and synchronized at a chosen period of $10ms$ with the simulator. Setpoints for each vehicle are listed thereafter:

- Damper preload (f_0);
- Left rear wheel torque;
- Right rear wheel torque;
- Steering rack translation.

5. Simulation results

5.1. Tests description

The ELK- and VDA-test trajectory is presented in Fig. 7. The road-train travels the ELK-test path at a speed of $45km.h^{-1}$.

Three configurations are considered: three-, five- and eight-module road-trains. The following tests are performed:

- ELK-test with three road-train configurations and three controllers: steering, damping and drive controllers;
- Straight and curved trajectories with end braking for an eight-module road-train, the most difficult case, with a single controller mixing steering and damping;

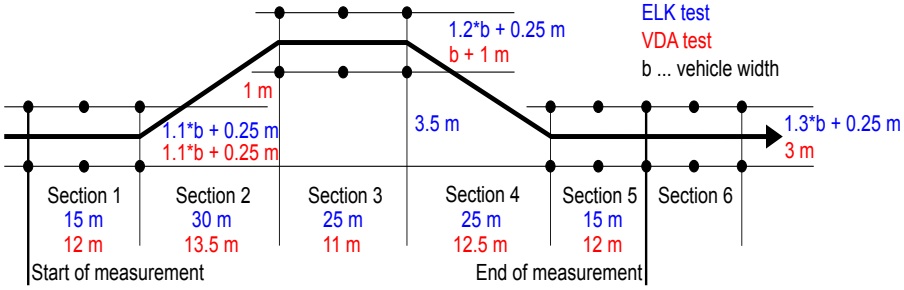

Figure 7: ELK- and VDA-test specification

- VDA-test, much more difficult than ELK-test for three road-train configurations and a single controller mixing steering and damping.

5.2. ELK-test

5.2.1. Steer controller

In road-train configuration, all steering wheels (except first vehicle front axle) are coupled with non-steered ones, as front axle of i^{th} vehicle is coupled with rear axle of $(i-1)^{th}$ vehicle. In practice, if steering angles are limited to a small value ($\pm 5°$), this kind of control is feasible. Moreover, steering velocity limits must be taken into account ($\pm 60°.s^{-1}$). Corrector synthesis was carried out around the road-train configuration for which all vehicles are aligned. This solution appeared to be more robust than a configuration-dependent synthesis.

LQR controller specifications are the following: $\mathbf{Q}_{\delta \mathbf{h}} = \mathbf{diag}\left(10^3, 10^{-5}, 10^3\right)$, $\mathbf{q}_{\delta\theta} = 10^3$, $\mathbf{R}_{\alpha} = 10^3 \mathbf{Id}_{n-1}$.

LQR controller specifications at $22km.h^{-1}$ and at $45km.h^{-1}$ for an eight-module road-train are plotted in Fig. 8. Column indices from 1 to 10 refer to posture error (high part of equation (11)), and column indices from 11 to 20 refer to velocity error (low part of equation (11)), while lines refer to steering angle setpoints computed by the controller.

Several remarks can be made:

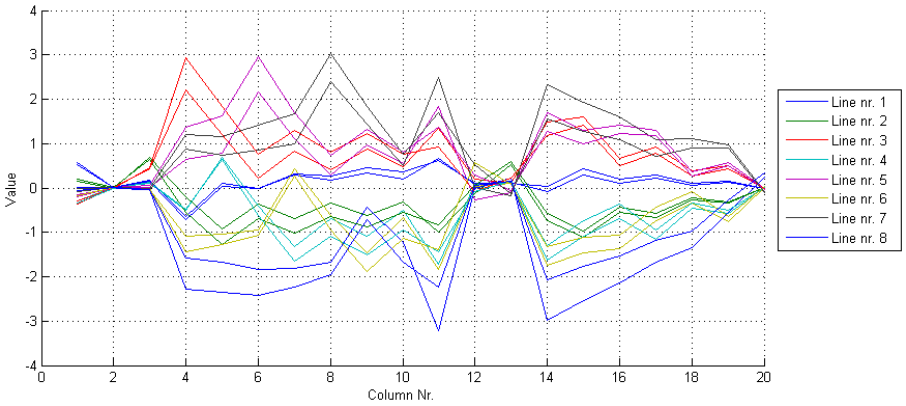

Figure 8: Comparison between two LQR controllers computed for $22km.h^{-1}$ and for $45km.h^{-1}$

- Even if some peaks associate a module orientation error (posture or velocity) with the steering angle of the same module, adjacent values for a same controller line cannot be forced to zero; which means that a diagonal controller structure cannot simply be extracted from that controller;
- A *Sparsity-Promoting LQR* method (see [19]) has been applied for controller complexity reduction, but without any significant result;
- Same lines for two very different velocities are quite close, making it easier to set up the controller at different velocities.

Test results are plotted in Fig. 9, Fig. 10 and Fig. 11 for three-, five- and eight-module road-trains respectively. Vertical axis is in $mm.s^{-1}$ for the leader's velocity (in red, divided by 3) and in mm for the different modules' trajectories. The following comments are made:

- The velocity is a little lower due to a low-level controller in charge of each wheel's velocity. This denotes a certain difficulty for the wheels to follow a prescribed velocity, especially during fast turns;
- Three- and five-module road-trains overshoots do not exceed $0.25m$, while eight-module road-train overshoot is about $0.5m$; the latter value could

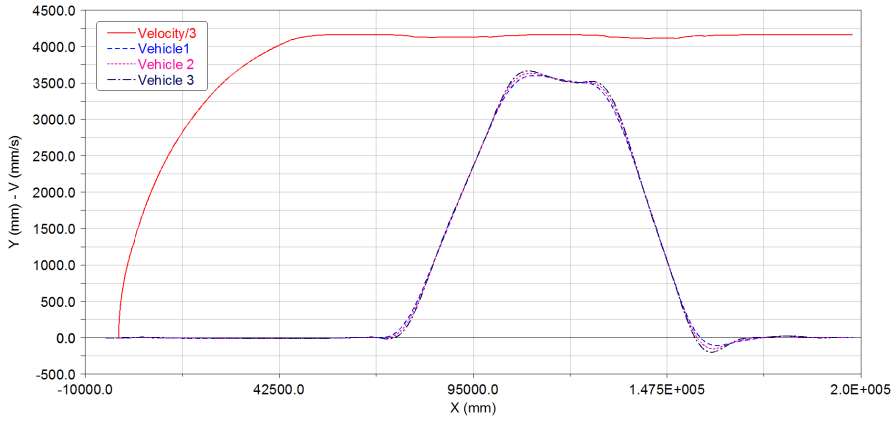

Figure 9: ELK-test for a three-module road-train and steering control

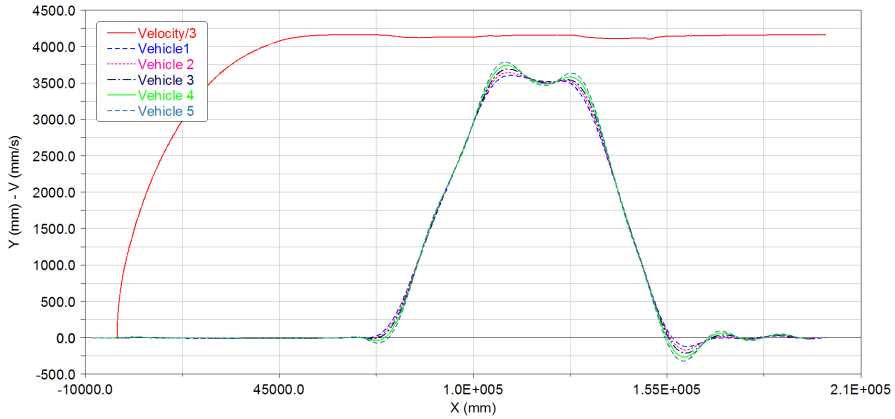

Figure 10: ELK-test for a five-module road-train and steering control

be reduced with a better trajectory tracking algorithm for the leader.

5.2.2. Damper controller

In a road-train configuration, referring to Fig. 1, 2, 3, $(\mathbf{a}_i)$ and $(\mathbf{c}_{i-1})$ frames positions are linked, and their relative orientation is actively damped. Even if the real system is equipped with linear dampers that are introducing geometric non-linearity, the control presented here is considering dampers rotation or moment. The only difficulty in this choice is the moment limitation which is

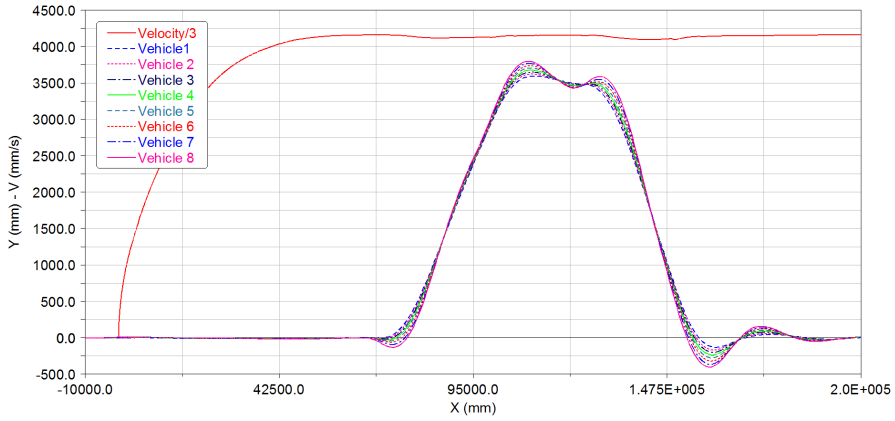

Figure 11: ELK-test for an eight-module road-train and steering control

varying according to the joint angle. However, since this variation is sufficiently small even during an ELK-test (less than 10°), a constant bounded moment limitation is considered for simulations.

The damper can be considered as a controlled dry friction. This control structure constraint could be taken into account within control synthesis, but in a rather complex way. In addition, computations have shown that LQR design leads to an overly conservative regulator, which is not sufficient to ensure stability. Instead, the following choice is made in this study: a non-constrained design and an a posteriori constrained control. Thus, a manually tuned diagonal proportional derivative control is designed. Inputs of the controller are joint gaps between the vehicle and the reference as well as their time derivative. Outputs are maximum oriented torques against joint motions. Control acts globally as a desired dry friction. Control constraints are as follows. Depending on the articulation angular error and angular rate signs, the corresponding torque may be non-active: $\tau_{\mathbf{c}_i} = 0$ if $\tau_{\mathbf{c}_i}.\dot{\theta}_{i-1,i} \geq 0$, with $\tau_{\mathbf{c}_i} = k_{p_i}\left(\theta_{i-1,i} - \theta_{i-1,i_{ref}}\right) + k_{d_i}\left(\dot{\theta}_{i-1,i} - \dot{\theta}_{i-1,i_{ref}}\right)$, k_{p_i} and k_{d_i} being the proportional and derivative gains respectively. Also, torques are saturated according to the nominal capacity of real dampers.

Best simulation results are finally obtained from the same controller specifica-

tion, meaning a 10^6 Proportional gain. Derivative gain did not appear to have a significant effect and is therefore maintained at zero.

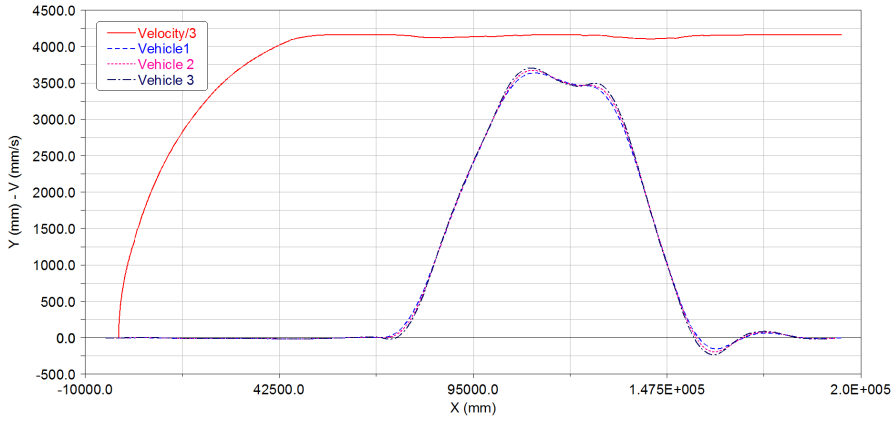

Figure 12: ELK-test for a three-module road-train and damper control

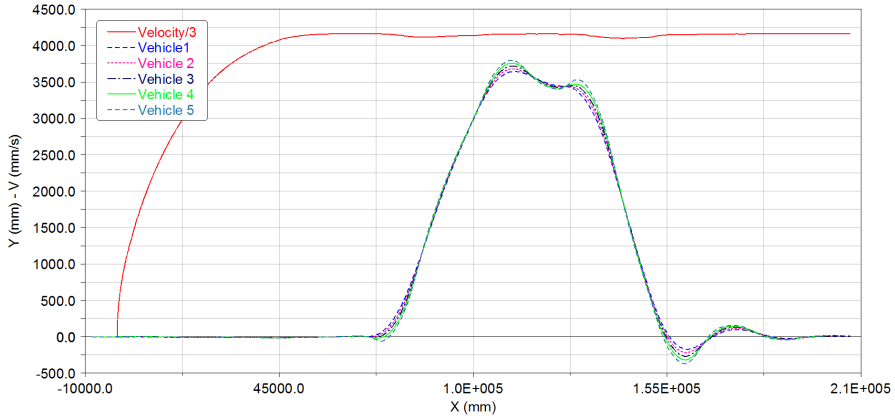

Figure 13: ELK-test for a five-module road-train and damper control

Damper control results are presented in Fig. 12, Fig. 13, Fig. 14. Overshoots are slightly higher: about $0.25m$ for a three-module road-train, $0.35m$ for a five-module road-train and $0.6m$ for an eight-module road-train.

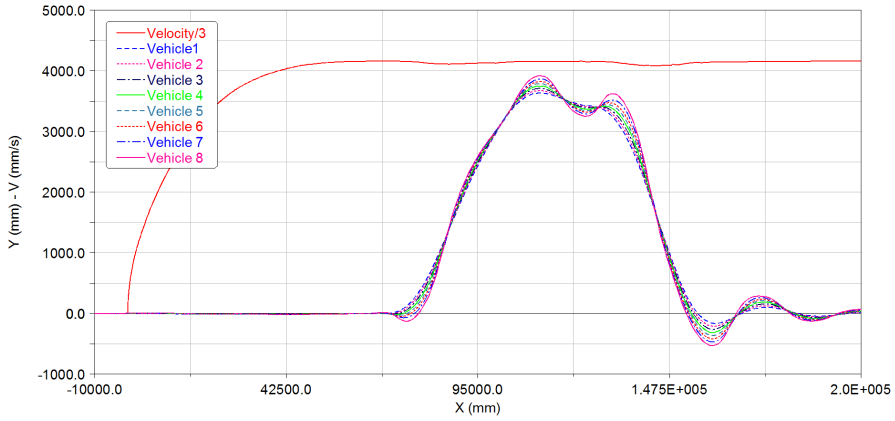

Figure 14: ELK-test for an eight-module road-train and damper control

5.2.3. Drive controller

With this controller, stabilization relies on power train control located on ($\mathbf{b}_i$) frames. Control can be two-way (positive and negative), but available actuator torque decreases considerably as velocity increases to $45km.h^{-1}$. To cope with this difficulty, rear wheel braking is also used, but only for deceleration.

As for the steering controller, a non-constrained LQR design is used and the control is constrained retrospectively. In the following, forces and torques are expressed at ground-tire interface, and not as wheel torques. Brake force limitation is expressed as a symmetrical maximum value independent of velocity, while actuators force limitation depends on velocity and, as a first approximation, this limitation is given by interpolation from zero velocity at maximum force to a $67km.h^{-1}$ velocity at maximum force.

Control constraints are the following, taking into account gear ratio and wheel radius for actuators: $F_{brake_{max}} = 3500N$, $F_{actuator_{max}} = 730N$ at $0km.h^{-1}$, and $F_{actuator_{max}} = 550N$ at $67km.h^{-1}$.

LQR controller parameters are the following: $\mathbf{Q}_{\delta\mathbf{h}} = \mathbf{diag}\left(10^{10}, 1.0, 10^{5}\right)$, $\mathbf{q}_{\delta\theta} = 10^{10}$, and $\mathbf{R}_{drive} = 10^{2}\mathbf{Id}_{n-1}$. The relative low value of $\mathbf{R}_{drive}$ is due to the capacity of high actuator-brake moments.

LQR controller specifications at $22km.h^{-1}$ and at $45km.h^{-1}$ for an eight-module

road-train are plotted in Fig. 15. Column indices from 1 to 10 refer to posture error (high part of equation (11)), and column indices from 11 to 20 refer to velocity error (low part of equation (11)), while lines refer to actuator-brake moments.

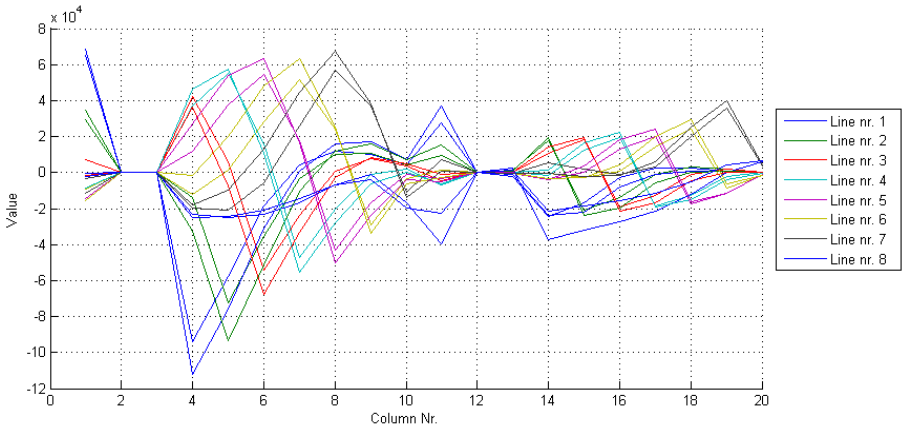

Figure 15: Comparison between two LQR controllers built for $22km.h^{-1}$ and for $45km.h^{-1}$

It can be noticed that:

- Peaks are well localized, and gain values are much less close to peaks, but several peaks can be noticed for the control of a same module, revealing a clear inter-modular coupling; however a *Sparsity-Promoting LQR* method could probably be efficient;
- Same lines for two very different velocities are quite close, making easier the controller computation at different velocities.

Drive control results are plotted in Fig. 16, Fig. 17 and Fig. 18 for three-, five- and eight-module road-trains respectively.

For an eight-module road-train, the velocity was reduced to $40.0km.h^{-1}$ (unstable over). While results are good enough for three- and five- modules road-trains, significant oscillations are noticeable for an eight-module road-train. This is

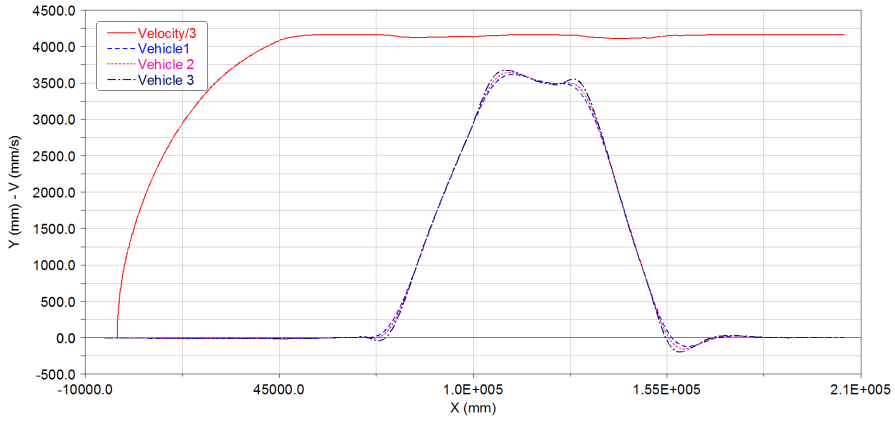

Figure 16: ELK-test for a three-module road-train and drive control

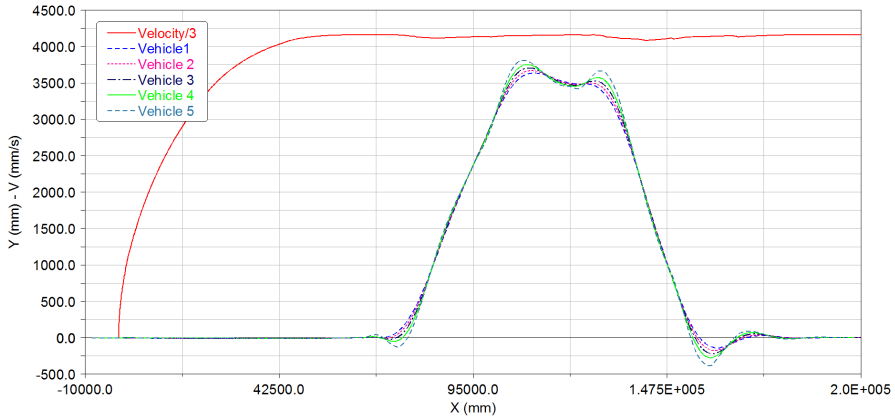

Figure 17: ELK-test for a five-module road-train and drive control

mainly due to low normal force exerted on inner wheels during turns, tending to reduce their action on the ground.

5.2.4. ELK-test conclusions

Overall, the three controllers meet an acceptable tolerance for nominal parameter setting. Realistic effector constraints have been taken into account. The strongest assumption is the sampling period of $10ms$. Steer and drive controllers can be combined linearly to compute a new stability controller, rather

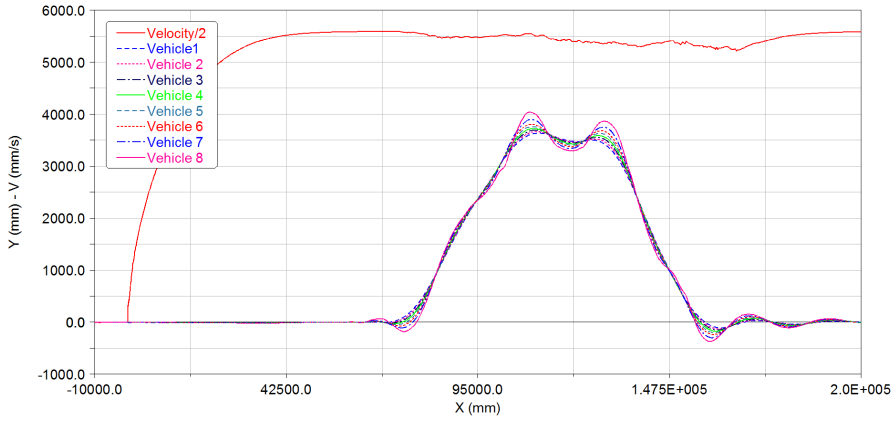

Figure 18: ELK-test for an eight-module road-train and drive control at $40.0km.h^{-1}$

than computing a new overall controller, including all inputs, still with a LQR approach. About the damper control, its simple addition may not destabilize the system because it is intrinsically passive (resistive force). The latter can be very useful when either or both steer and drive controllers are no longer available. For example, in the event of a skid, stability should only be based on damper control.

5.3. Braking on straight trajectory

For this and subsequent tests, the road-train controller is mixing steering and damper controls. The motors' power is dedicated to driving and braking. Here, only the eight-module road-train has been considered at about $60km.h^{-1}$. The result is given in Fig. 19. Deceleration is about $4.8m.s^{-2}$ and gap is negligible ($< 0.1m$).

5.4. Turning and Braking

After reaching $45km.h^{-1}$, an eight-module road-train turns and follows a $40m$ radius circular trajectory, then brakes. Lateral acceleration during the turn is about $4.0m.s^{-2}$. Results are illustrated in Fig. 20. For the last vehicle, the gap can be estimated at $0.9m$. At the end of the trajectory, braking at $4.5m.s^{-2}$ does not result in a larger gap.

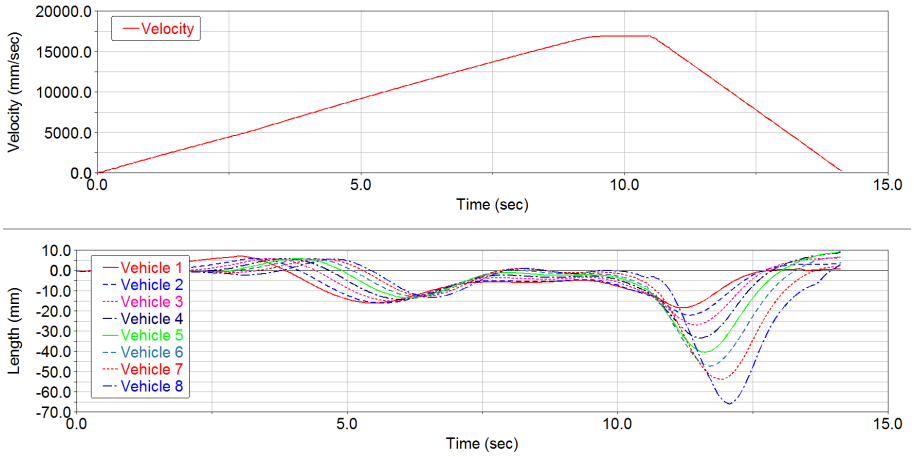

Figure 19: Above: Velocity profile in $mm.s^{-1}$. Beneath: Gap in mm

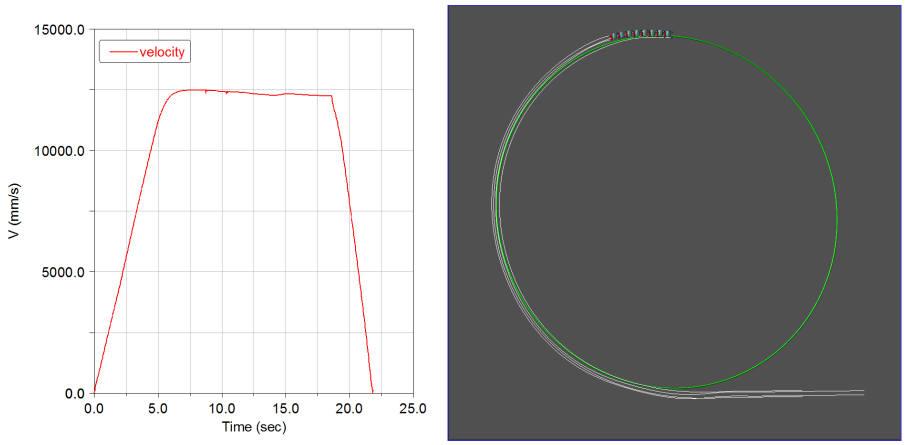

Figure 20: Left: Velocity profile in $mm.s^{-1}$. Right: Reference circle (green) and first and last module traces (white)

5.5. VDA-test

475 VDA-test is similar to an ELK-test, but far more demanding. As turns are twice as sharp, this test is likely to disturb the system with four times more energy. Results for three-, five- and eight-module road-trains are illustrated in Fig. 21, Fig. 22 and Fig. 23 respectively. Velocity is about $40km.h^{-1}$.

The test is successful with three- and five-module road-trains; the eight-module

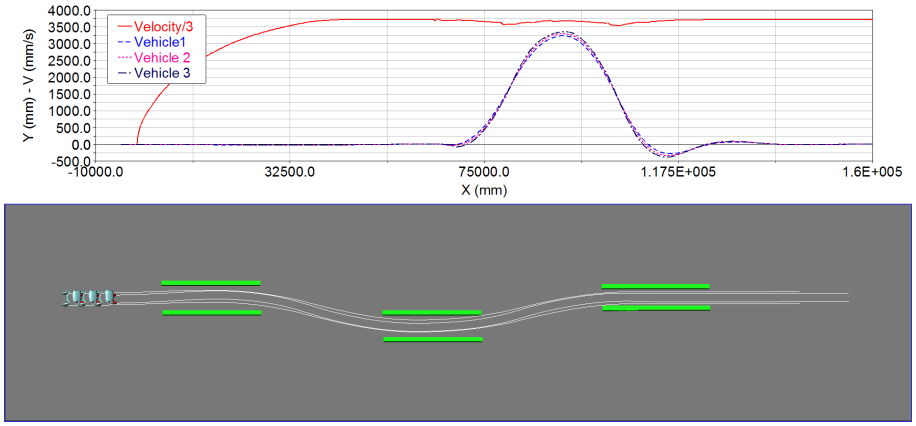

Figure 21: VDA-test for a three-module road-train

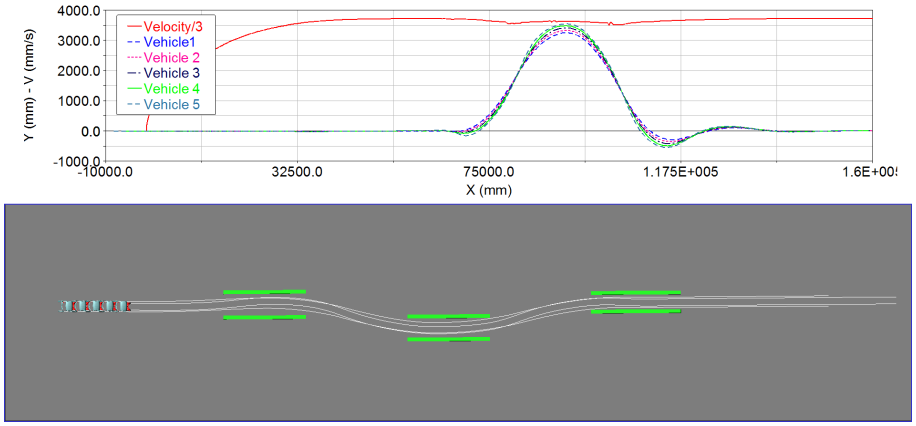

Figure 22: VDA-test for a five-module road-train

480 road-train is close to passing the test, but a gap of $0.3m$ is still noted. Other additional simulations show that for such demanding tests, damper control is predominant, while steering control is mainly efficient for small corrections.

During VDA-test, coupling wrenches between vehicles are quite large. These 485 wrenches are higher for an eight-module road-train, especially between fifth and sixth vehicles. These forces, measured at coupling bushings, are plotted in Fig. 24. A maximum longitudinal force of about $20000N$ can be observed in

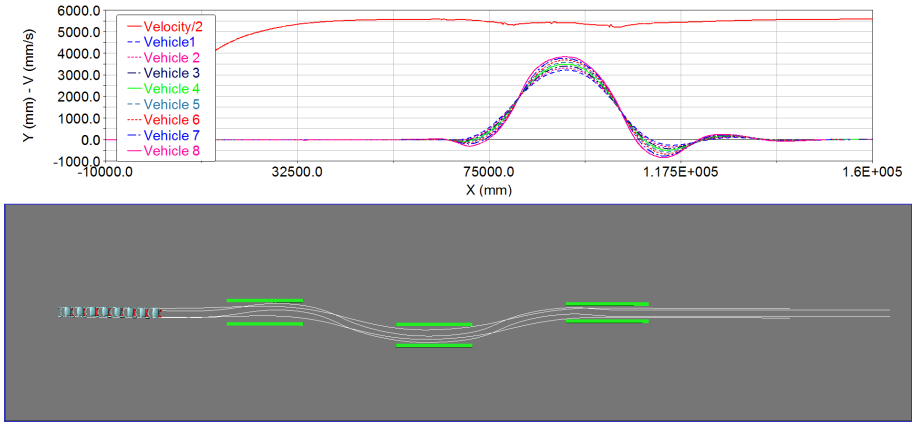

Figure 23: VDA-test for an eight-module road-train (video)

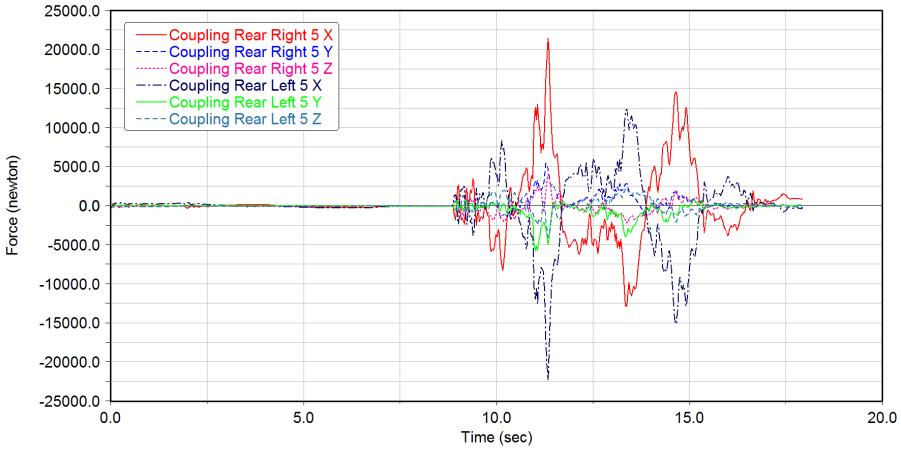

Figure 24: Coupling bushing forces

this figure. A maximum moment of about $6000N.m$ is deduced from this force, using the bushing position.

6. Experimental results

6.1. Experimental system description

Experimental trials were conducted on a road-train composed of five ESPRIT light-weight category electric vehicles; see Fig. 25. The first two vehicles are

designed with a steel structure, while the next three vehicles are designed with an aluminium structure, and they have the final covering intended for its public use. Despite these differences, all vehicles have approximately the same mass of $700kg$ and have exactly the same geometric and kinematic properties that are used for the simulation. Damper force sensors are installed to provide a force measurement for damper control, rather than the sign of the articulation speed. This is done for better reactivity, considering the force measurement before the articulation movement starts.

Figure 25: The 5 ESPRIT vehicle road-train

The driving is done by an operator in the front vehicle, using manual control interfaces: steering wheel and pedals. The towed vehicles communication with the front one is done through CAN bus for an autonomous control.

The software structure of the on-board controller of each vehicle is separated in four main parts: a state-machine, a stabilisation command law, a data dispatcher and an error management and mitigation module. Tests were performed on these four separate parts and the timing behaviour of these parts was analysed [20].

The road-train is stabilized by using the following actuators:

- Front steering of towed vehicles - Their angle setpoint is between $-5deg$ and $5deg$, with also an angular speed between $-60deg/s$ and $60deg/s$. The value of the steering angle is computed by using an LQR controller.
- Damper of towed vehicles - Their resistive force setpoint is computed

by using a selective proportional derivative controller on the articulation torque.

- Wheel motors have limited power and are necessary for propulsion. They are therefore not used for stabilization.

Also, the following sensors are used:

- An IMU sensor in master front vehicle, for yaw angle and yaw rate measurement.
- Rear wheels odometers of master front vehicle, for position estimation.
- Articulation angle sensor of towed vehicles, for articulation angle (analogic filter at $10Hz$) and articulation angular speed measurements.
- Damper force sensor of towed vehicles, for damper force sign measurement.

6.2. VDA test results

Tests were carried out on a track dedicated to car tests. The weather was fine without rain during all the tests, so the grip conditions were correct ($2.4bar$ tire pressure).

First, by using the steering, the behavior of the vehicle had a lack of stability. Indeed, the steering of towed vehicles seemed to turn too much. Because of that, the vehicle was even hard to stabilize in straight line. This was due to the CAN communication time too important, and so the stabilization control was then limited to the damper.

Then, changes were made to the settings of the control algorithm by adding a residual damping force value of $1000N$, setting the maximum damping force value to $39600N$ and adapting the reference model used for the 1^{st} vehicle with EKF filtering to avoid a destabilizing coupling that may occur between the reference and the vehicle. The wheel traction torque of each towed vehicle was also reduced by a factor of 0.8 compared to the vehicle in front.

A VDA test with the 5 vehicle road-train at $40km/h$ was then carried out

under satisfactory conditions. The Fig. 26 is a picture of the road-train at the beginning of the second turn at $t = 50690.4s$ when the cumulative angular errors of articulations are the most important, and the Fig. 27 displays the state of the real road-train in blue and of its reference model in yellow at that time, with the first vehicle at the bottom right.

Figure 26: Road-train at the beginning of the second turn (video)

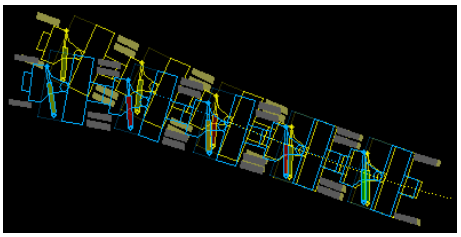

Figure 27: Monitoring of the road-train state

Odometric measurement of the position of the front axle centre of the first vehicle is plotted in Fig. 28 below. The two turns of the VDA test are visible at positions $y = 60m$ and $y = 90m$, respectively at times $t = 50687s$ and $t = 50690s$. For this test, the road-train reaches its maximum speed at the beginning of the first turn, then the driver stops accelerating and allows this speed to decrease until the end of the trajectory (see Fig. 29). For this test, a speed of $11.1m/s$ is reached, which corresponds to $40km/h$.

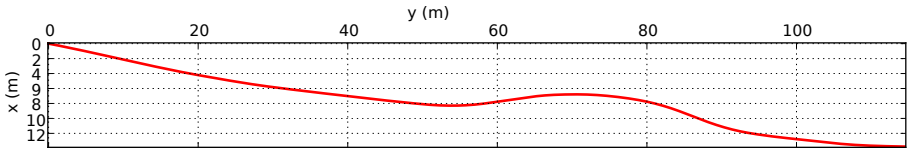

Figure 28: First vehicle front axle trajectory

Data of the output error vector (11) used for the stabilization control, by using only the towed vehicles articulation damper, are plotted in Fig. 30 and 31 below by zooming in as the two turns pass. Otherwise, these errors always remain almost zero. The first left turn produces a positive angular error while the second

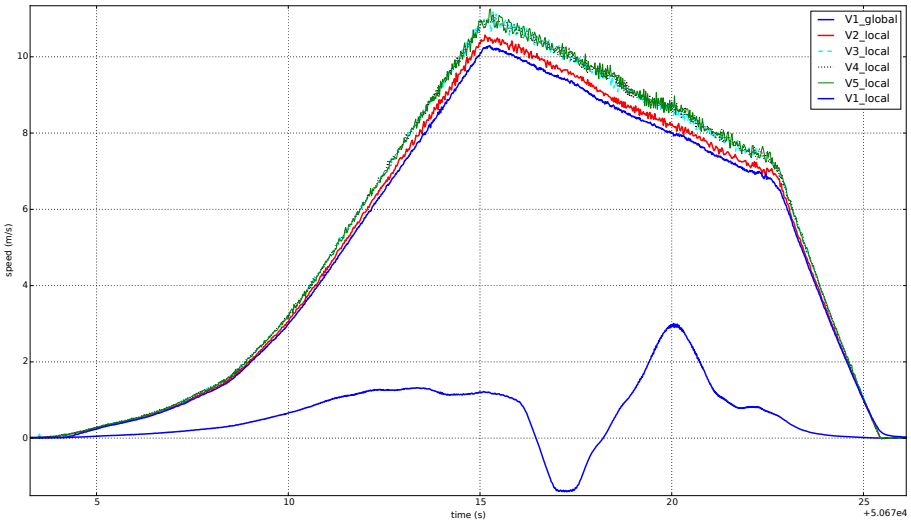

Figure 29: Front vehicle speed in global frame and vehicles speed in local frame

turn produces a negative angular error at the first articulation (red curve in Fig. 30). Then this error spreads to other articulations with a sign that may vary from one articulation to another. Articulation angles errors are oscillating during the two turns with reasonable maximum amplitudes of θ_{23} error (dotted black curve in Fig. 30) of $+0.14rad$ $(+8.02deg)$ and $-0.24rad$ $(-13.75deg)$, respectively after the first and after the second turn manoeuvres. And the maximum $\dot{\theta}_{23}$ errors (dotted black curve in Fig. 31) are $+0.44rad/s$ $(+25.21deg/s)$ and $+0.48rad/s$ $(+27.50deg/s)$, also respectively after the first and after the second turn manoeuvres. The largest rotational amplitudes therefore occur on the fourth vehicle, and then on the fifth and last vehicle.

Then, the parameters defining the damper control are plotted below for each articulation of the four towed vehicles of the road-train in Fig. 32, Fig. 33, Fig. 34 and Fig. 35. The blue curve corresponds to the angular error already plotted in Fig. 30. The dotted black curve corresponds to the sign of the force measured at the articulation. When these two curves are of opposite sign, the green selection curve is 1, which means that a non-zero U_{damp} control of the damper is computed (dashed cyan curve) and translated to a positive resistive

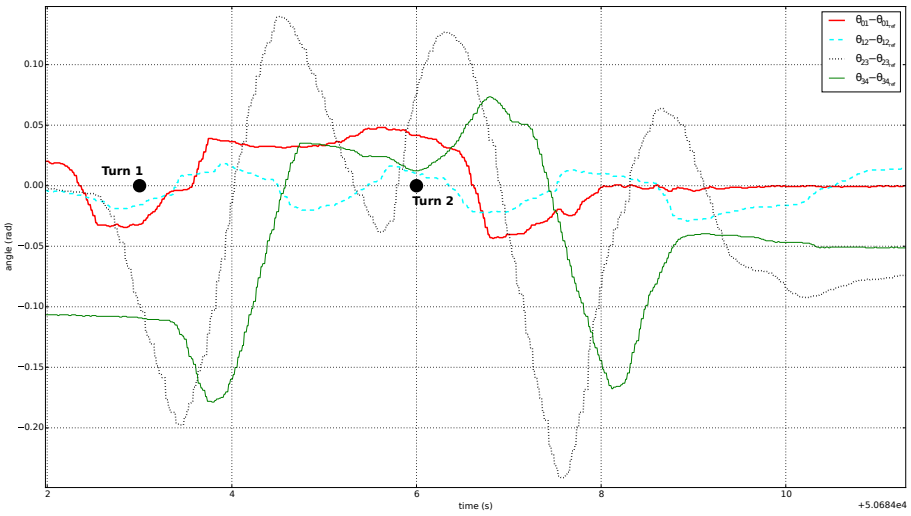

Figure 30: Articulation angle error data

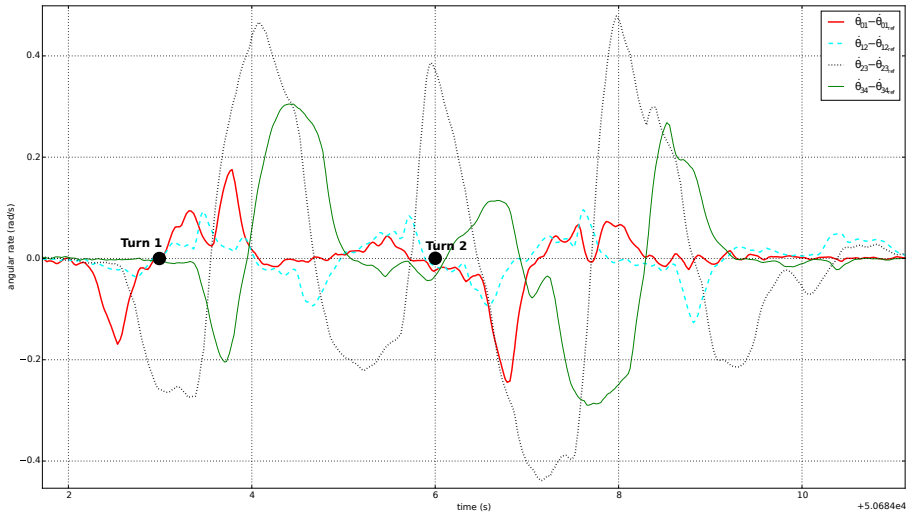

Figure 31: Articulation angular rate error data

575 force to be applied by the damper. Otherwise, the selection curve is 0 and the damper is free. The red curve corresponds to the angular velocity error already plotted in Fig. 31, which could be taken into account in addition to the blue curve to define the control selection threshold and the control value U_{damp}.

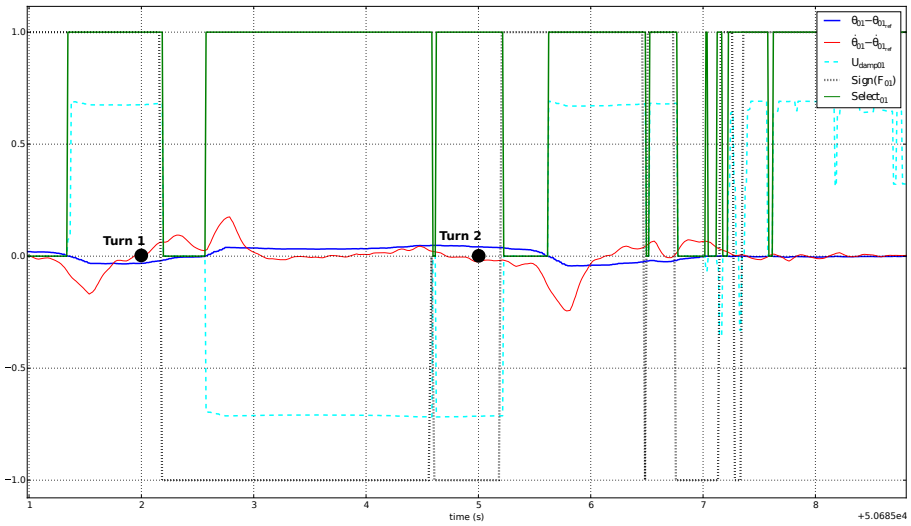

Figure 32: Damper control data for θ_{01} articulation

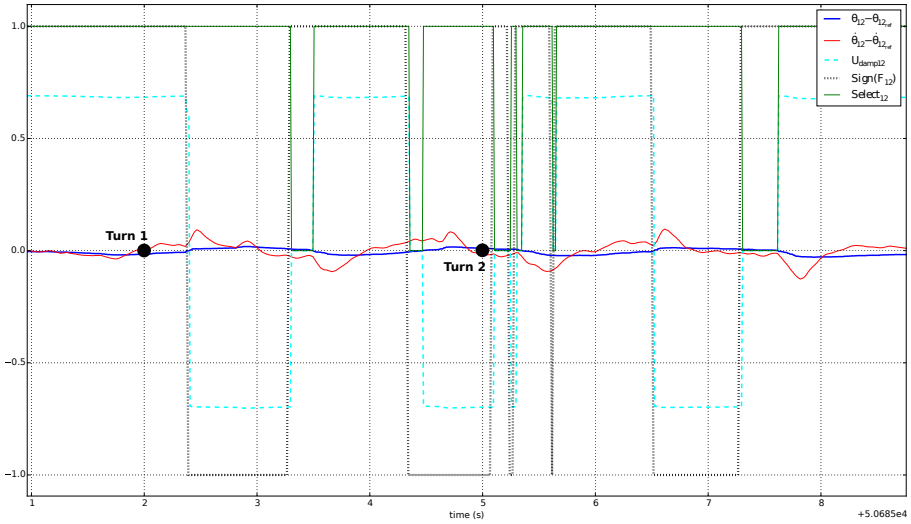

Figure 33: Damper control data for θ_{12} articulation

The two turns of the VDA test occurring respectively at times $t = 50687s$ and $t = 50690s$, the maximum of angular error and angular velocity error occur near these values, and consequently a high damper control value is applied. Outside these two turns, a damper control is applied to prevent an unwanted

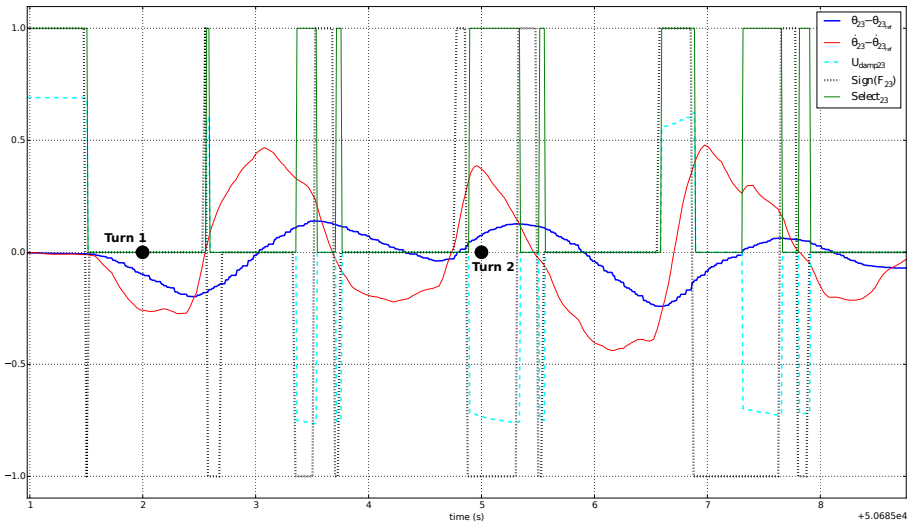

Figure 34: Damper control data for θ_{23} articulation

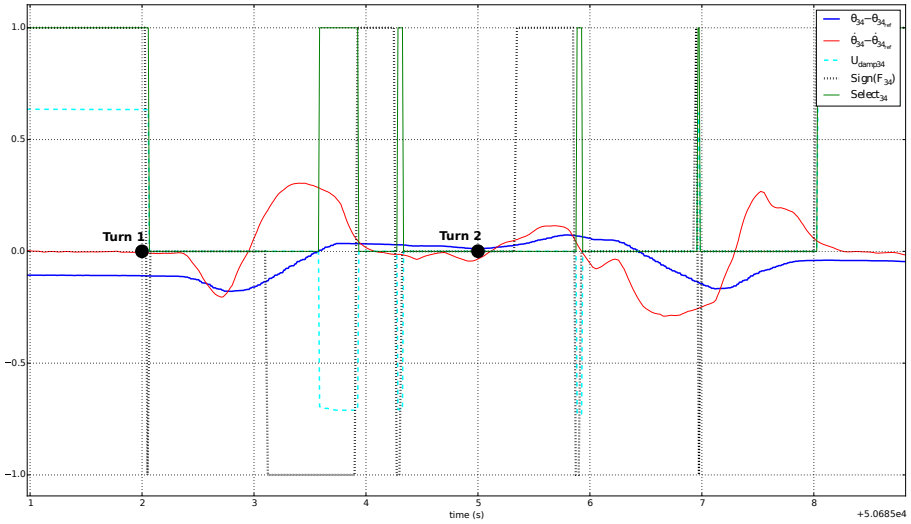

Figure 35: Damper control data for θ_{34} articulation

articulation angle from increasing. In the case of θ_{01} articulation (see Fig. 32), oscillating controls (dashed cyan curve) are observed during the turns and after to maintain the articulation angle around a zero angle. A similar behaviour is observed for θ_{12} articulation (see Fig. 33) with almost continuous damper control

throughout the VDA test. The control of θ_{23} articulation (see Fig. 34) is more punctual, between the two turns and during the second turn, because the sign of the angle of this articulation does not always allow the control to be activated. This phenomenon is even more visible for the control of θ_{34} articulation (see Fig. 35), for which the damper control is activated between the two turns. Finally, by controlling the damper, the oscillation of the articulation angles is quickly dampened, all of which return to zero after $t = 50693s$.

7. Conclusions

A modular 2D dynamic model was developed and implemented to design and evaluate three controllers to ensure the dynamic stabilization of a road-train of vehicles: steering, drive and damping controllers. These three controllers can be used together, the first two being combined linearly (sum of weights must be equal to one) and the third simply added. The first two controllers can be tuned automatically, applying an LQR approach based on a linearized model around a single aligned configuration. For the third, a constant high gain can be applied in all cases.

Main conclusions and future improvements are the following. As brakes are used for drive control, their accuracy will have an impact on this control effectiveness. For a damper control, it is necessary to know the motion direction of inter-module joint angles, via angular velocity sign or preferably via force direction measurement undergone by the damper. The driver only controls first module's steering, which has been manually tuned for each test considered not to be too aggressive. The driver is an active component of the controller. In case of incorrect behavior, for example too much lag reaction, he may destabilize the vehicle. In particular, kinematic reference is directly linked to the first module steering. Such a choice does not require to know the driver's intention. Even in sharp trajectories, this reference behaves well. But once the oscillations become more significant, a destabilizing coupling may appear between the reference and the vehicle. That is why, a filtering of the reference behaviour was proposed.

Also, all controllers proposed are only based on proprioceptive state observation. These three controllers have been validated in a realistic 3D simulated environment, that takes into account complex dynamic effects as close as possible to a real system, with a road-train of up to eight articulated vehicles.

Then tests were conducted in real conditions on a five-vehicle road-train. The drive controller using vehicle brakes and engines was not used on real vehicles because the use of these actuators was already fully necessary to ensure the traction and safety of the road-train. The second controller using vehicle steering has shown limited effectiveness in real tests due to inter-vehicle communication issues. Indeed, the VDA test demands a lot of the vehicle's dynamics, and requires excellent reactivity. Finally, the third method, which uses the dampers of the central articulation of vehicles, has shown good performance and allowed the VDA-test to be successfully passed. In order to further improve these results, two options could be investigated. Technically, the CAN communication network used could be replaced by a more efficient means of communication, such as an Ethernet solution. Another possibility would be to reconsider the control strategy at the local level to minimize the need for inter-vehicle communication. However, this second solution is not a trivial one, as vehicles are highly interdependent. Finally, there was no use of grip loss detector, which would be helpful to better modulate control setpoints.

Acknowledgments

This research and development work was carried out in the scope of the Easily diStributed Personal RapId Transit (ESPRIT) project. This project has received funding from the *European Union's Horizon 2020 research and innovation program* under grant agreement N°653395.

References

[1] ESPRIT, Easily diStributed Personal RapId Transit project (2017).
URL `http://www.esprit-transport-system.eu/`

[2] V. Cervantes, P. Davidson, H. Porter, Developing a new mobility as a service concept, in: European Transport Conference (ETC), Barcelona, Spain, 2017, pp. 1–7.
URL https://aetransport.org/public/downloads/8Mxcv/5573-59ba49dc7569c.pdf

[3] T. Bendixson, M. G. Richards, Witkar: Amsterdam's self-drive hire city car, Transportation 5 (1) (1976) 63–72. doi:10.1007/BF00165248.
URL https://link.springer.com/article/10.1007/BF00165248

[4] CHISPA electric public cars.
URL https://sites.google.com/site/chispapubliccarsystem/

[5] M. Yksel, S. Losch, S. Kroffke, M. Rohn, F. Kirchner, BLDC wheel hub motor and motor controller performance test of a concept electric robotic vehicle in HIL according to real driving characteristics, in: 2015 9th International Conference on Electrical and Electronics Engineering (ELECO), 2015, pp. 613–617. doi:10.1109/ELECO.2015.7394578.

[6] P. Fairley, Car sharing could be the EV's killer app, IEEE Spectrum 50 (9) (2013) 14–15. doi:10.1109/MSPEC.2013.6587173.

[7] L. Cheng, Y. Xu, Design of intelligent control system for electric vehicle road train, in: Proceedings of the 10th World Congress on Intelligent Control and Automation, 2012, pp. 3958–3961. doi:10.1109/WCICA.2012.6359134.

[8] P. Morin, C. Samson, Feedback control of the general two-trailers system with the Transverse Function approach, in: 2012 IEEE 51st IEEE Conference on Decision and Control (CDC), 2012, pp. 1003–1010. doi:10.1109/CDC.2012.6427071.

[9] J. M. Contet, F. Gechter, P. Gruer, A. Koukam, Application of Reactive Multiagent System to Linear Vehicle Platoon, in: 19th IEEE International

Conference on Tools with Artificial Intelligence(ICTAI 2007), Vol. 2, 2007, pp. 67–70. doi:10.1109/ICTAI.2007.56.

[10] H. Hao, P. Barooah, Stability and robustness of large platoons of vehicles with double-integrator models and nearest neighbor interaction, International Journal of Robust and Nonlinear Control 23 (18) (2013) 2097–2122.

[11] P. de Larminat, Automatique : Commande des systèmes linéaires, Hermes Science Publications, 1993.

[12] R. M. Murray, Z. Li, S. S. Sastry, A Mathematical Introduction to Robotic Manipulation, CRC Press, Boca Raton, 1994.

[13] G. RILL, First order tire dynamics, in: Proceedings of the III European conference on computational mechanics solids, structures and coupled problems in engineering, Vol. vol. 58, Springer Netherlands, Lisbon, Portugal, 2006, p. 776. doi:10.1007/1-4020-5370-3_776.

[14] W. Hirschberg, G. Rill, H. Weinfurter, Tire model TMeasy, VEHICLE SYSTEM DYNAMICS 45 (S) (2007) 101–119. doi:10.1080/00423110701776284.

[15] G. C. Goodwin, K. S. Sin, Adaptive filtering prediction and control., Prentice-Hall Information and System Sciences Series. Englewood Cliffs, New Jersey 07632: Prentice-Hall, Inc. XII., p. 293 (1984).

[16] E. Todorov, Optimal Control Theory, book chapter to appear in Bayesian Brain, Doya, K. (ed), MIT Press, 2006, page 16.
URL https://homes.cs.washington.edu/~todorov/courses/amath579/Todorov_chapter.pdf

[17] ADAMS, The multibody dynamics simulation solution, http://www.mscsoftware.com/product/adams (2017).
URL http://www.mscsoftware.com/product/adams

[18] H. Pacejka, Tyre and vehicle dynamics, Butterworth Heinemann, 2002.

[19] F. Lin, M. Fardad, M. R. Jovanovic, Design of optimal sparse feedback gains via the alternating direction method of multipliers, IEEE Transactions on Automatic Control 58 (9) (2013) 2426–2431. doi:10.1109/TAC.2013.2257618.

[20] N. Gobillot, E. Lucet, Esprit: Overview of the vehicles road-train real-time architecture, in: Proceedings of ERTS^2 2018 - 9$^{\text{th}}$ European Congress Embedded Real Time Software and Systems, Toulouse, France, 2018.